Axin proteolysis by Iduna is required for the regulation of stem cell proliferation and intestinal homeostasis in *Drosophila*

Yetis Gultekin[1] and Hermann Steller[1]*

[1]Strang Laboratory of Apoptosis and Cancer Biology, The Rockefeller University, 1230 York Avenue, New York, NY 10065, USA.

***Corresponding author:**
E-mail: steller@rockefeller.edu. Strang Laboratory of Apoptosis and Cancer Biology, The Rockefeller University, 1230 York Avenue, New York, NY 10065, USA. Tel: (212) 327-7075.

Running Title: Iduna regulates stem cell proliferation and intestinal homeostasis

Keywords: wingless, Axin, ADP-ribosylation, protein degradation, ubiquitin E3 ligase, stem cells.

Abstract

The self-renewal of intestinal stem cell is controlled by Wingless/Wnt-β catenin signaling both in *Drosophila* and mammals. Since Axin is a rate-limiting factor in Wingless signaling its regulation is essential. Iduna is an evolutionarily conserved ubiquitin E3 ligase that has been identified as a critical regulator for degradation of ADP-ribosylated Axin and thus of Wnt/β-catenin signaling. However, its physiological significance remains to be demonstrated. Here, we generated loss-of-function mutants of *Iduna* to investigate its physiological role in *Drosophila*. Genetic depletion of *Iduna* causes the accumulation of both Tankyrase and Axin. Increase of Axin protein in enterocytes non-autonomously enhanced stem cell divisions in the *Drosophila* midgut. Enterocytes secreted Unpaired and thereby stimulated the activity of the JAK-STAT pathway in intestinal stem cells. A decrease in *Axin* gene expression suppressed both the over-proliferation of stem cells and restored their numbers to normal levels in *Iduna* mutants. These findings suggest that Iduna-mediated regulation of Axin proteolysis is essential to maintain tissue homeostasis in the *Drosophila* midgut.

41 **Introduction**

42 The evolutionarily conserved Wnt/β-catenin signaling pathway is a main regulator of
43 animal development. It controls proliferation, differentiation and regeneration of adult
44 tissues (Herr et al., 2012; Nusse and Clevers, 2017). The Wingless pathway is also
45 involved in adult tissue self-renewal in *Drosophila* (Lin et al., 2008). Genetic depletion of
46 proteins in the Wingless pathway, such as *Tcf*, *arr, dsh* and *pygo,* leads to inhibition of
47 Wingless signaling activation which in turn causes over-proliferation of stem cells in the
48 *Drosophila* midgut (Kramp et al., 2002; Wang et al., 2016a and 2016b; Tian et al.,
49 2016). However, inactivation of Wnt signaling in the small intestine of mice decreases
50 the proliferative potential of stem cells (Fevr et al., 2007; Korinek et al., 1998). On the
51 other hand, mutations resulting in the over-activation of the Wnt/β-catenin pathway
52 promote tumorigenesis (Clevers and Russe, 2012; Andreu et al., 2005; Korinek et al.,
53 1997 and 1998; Morin et al., 1997). For instance, mutations on *adenomatous polyposis*
54 *coli (APC)* gene cause a hereditary colorectal cancer syndrome called familial
55 adenomatous polyposis (Kinzler et al., 1991; Nishisho et al., 1991). Axin loss-of-function
56 mutations are found in hepatocellular carcinomas, while oncogenic β-catenin mutations
57 are described in colon cancer and melanoma (Rubinfeld et al., 1997). Consequently,
58 intense efforts have been made to target this pathway for therapeutic purposes (Clevers
59 and Russe, 2012).

60 A key feature of the Wnt/β-catenin pathway is the regulated proteolysis of the
61 downstream effector β-catenin by the β-catenin degradation complex. The principal
62 components of this complex are adenomatous polyposis coli (APC), Axin and Glycogen
63 synthase kinase 3β (GSK3β) (Kramps et al., 2002; Hamada et al., 1999; Salic et al.,

64 2000; Lee at al., 2003). Axin, a critical scaffold protein in the β-catenin degradation
65 complex, is the rate-limiting factor of Wnt signaling and its protein levels are regulated
66 by the Ubiquitin-Proteasome System (UPS) (Li et al., 2012). Axin is targeted for
67 degradation by the combined action of the poly-ADP-ribose polymerase Tankyrase
68 (TNKS) and the ubiquitin E3-ligase Iduna/Ring finger protein 146 (RNF146) (Zhang et
69 al., 2011). Both genetic and pharmacological studies suggest that UPS-dependent
70 degradation of Axin occurs in a specific temporal order. Iduna initially exists in an
71 inactive state, but binding to its iso- or poly-ADP-ribosylated targets causes allosteric
72 activation of the enzyme (DaRosa et al., 2015). In the first step, TNKS binds to Axin and
73 ADP-ribosylates Axin using NAD^+. Then, Iduna recognizes and binds to ADP-
74 ribosylated Axin via its WWE domain and poly-ubiquitylates Axin. Following the ADP-
75 ribosylation and ubiquitination, post-translationally modified Axin is rapidly degraded by
76 the proteasome (DaRosa et al., 2015; Wang et al., 2016a and 2016b; Croy et al., 2016;
77 Callow et al., 2011). This tight control suggests an important function for Iduna to
78 regulate the Wnt-β catenin pathway.

79 Since the stability of Axin is partially regulated by TNKS-mediated ADP ribosylation,
80 specific small-molecule inhibitors have been developed to inhibit Wnt-signaling (Lu et
81 al., 2009; Huang et al., 2009). For example, XAV939 targets the ADP-ribose
82 polymerase activity of TNKS and increases Axin levels, which in turn destabilizes β-
83 catenin to inhibit Wnt signaling (Huang et al., 2009). There are two TNKS isoforms in
84 mammalian cells (Hsiao et al., 2006). *Tnks1*$^{-/-}$ and *Tnks2*$^{-/-}$ mice are overall normal;
85 however, double knock-out of *Tnks*$^{1/2}$ causes early embryonic lethality, which indicates
86 their redundancy in mouse development (Hsiao et al., 2006; Chiang et al., 2008). On

87 the other hand, inactivation of the single *Drosophila Tnks* gene produces viable flies that
88 have slightly increased Axin levels and abnormal proliferation of intestinal stem cells,
89 but otherwise display no overt defects (Wang et al., 2016a and 2016b; Feng et al.,
90 2014; Yang et al., 2016; Tian et al., 2016). On the other hand, the exact physiological
91 function of Iduna remains to be determined. In order to address this question, we
92 generated and characterized *Drosophila* Iduna loss-of-function mutants and
93 demonstrate a critical function of this pathway for stem cells in the *Drosophila* intestinal
94 tract.

95 The *Drosophila* genomes encode four isoforms of *CG8786/Iduna/RNF146*, which is
96 evolutionarily conserved from *Drosophila* to human. In this study, we concentrated on
97 the physiological function of Iduna in the adult *Drosophila* midgut, which shares several
98 striking similarities with the mammalian small intestine but offers greater anatomical and
99 genetic accessibility (Micchelli et al., 2005; Ohlstein et al., 2005; Markstein et al., 2013).
100 Under normal conditions, Wingless signaling controls stem cell proliferation and cell fate
101 specification in adult midgut (Tian et al., 2016). Here, we show that Iduna has a
102 physiological function to regulate the proteolysis of both TNKS and Axin. Inactivation of
103 *Iduna* results in increased numbers of midgut stem cells and progenitors due to over-
104 proliferation. We find that Axin accumulation in enterocytes promotes the secretion of
105 Unpaired, a cytokine that binds to the Domeless receptor and activates the JAK-STAT
106 pathway in stem cells and thereby promotes stem cell division. Significantly, reducing
107 *Axin* expression by half restores the numbers of ISC. These findings indicate that
108 regulation of Axin proteolysis by Iduna is necessary to control intestinal homeostasis in

109 *Drosophila,* and it provides physiological evidence for the idea that the function of Tnks

110 and Iduna/RNF146 is tightly coupled.

111

112 **Results**

113 **Iduna plays a role in Axin degradation:** To examine the *in vivo* function of *Drosophila*
114 Iduna, CRISPR-Cas9 genome editing was used to generate *Iduna* mutants. *Iduna* is
115 located on the 3rd chromosome of *Drosophila*. We designed a specific guide RNA that
116 targets *Iduna*`s first exon and identified two mutant alleles by Sanger sequencing:
117 $Iduna^{17}$ and $Iduna^{78}$, which have 4-nucleotides and 2-nucleotides deletions, respectively
118 (Fig 1A). These deletions are close to the translation start side of *Iduna*. Next we
119 assessed the levels of mRNA and protein expression in these mutants. Using reverse
120 transcript PCR analysis, we found significantly reduced amounts of *Iduna* transcripts in
121 the $Iduna^{78}$ mutant. On the other hand, we were unable to detect any *Iduna B* and *C/G*
122 transcripts in the $Iduna^{17}$ allele (Fig S1A). Moreover, no Iduna protein was detected in
123 either of these mutants, indicating that they represent Null-mutations (Fig 1B). Finally,
124 genetic analyses of these alleles in trans to a larger deletion (see below) indicate that
125 both alleles are complete loss-of-function mutations. *Iduna* mutants were crossed to
126 *Drosophila* deficiency lines [Df(3L) Exel6135, Df(3L) ED228)] and also to each other
127 and all combinations were viable as trans-heterozygotes.

128 We examined the larval development of *Iduna* mutants and Oregon R but did not
129 observe any differences in the numbers of hatched eggs (Fig S1B-C), pupated larvae
130 and enclosed adult *Drosophila* (Fig S1D) between *Iduna* mutants and wild type. *Iduna*-
131 Null adult flies had no overt morphological defects when compared with wild type
132 controls. However they displayed increased mortality upon nutrient deprivation. We
133 challenged mutant and wild type adult females with a 5% sucrose diet at 28^0C. Two-

134 day old adult females were placed on 5% sucrose diet at 28°C. Mutant flies died within
135 17 days, while 70-80% of wild type flies were still viable at this time (Fig 1C).
136

137 Iduna is one of the key components of the machinery that degrades Axin whose ADP-
138 ribosylation by TNKS is important for mammalian Wnt-β catenin signaling (Li at al.,
139 2012). We detected increased levels of endogenous Axin in the lysates from *Iduna*
140 mutants midguts compared to controls (Fig 2A). Mammalian Iduna recognizes both
141 ADP-ribosylated (ADPR) TNKS and Axin via the R163 residue in its WWE domain
142 (Zhang et al., 2011). The R163 residue is conserved in evolution and corresponds to
143 R252 in the *Drosophila* WWE domain (Fig 2B). To examine the level of endogenous
144 ADPR-Axin in *Iduna* mutants, ADPR-Axin was pulled down with wild type-WWE or
145 R252A-WWE-mutant recombinant proteins (Fig 2C). This analysis revealed that *Iduna*
146 mutants had a more than two-fold increase in ADPR-Axin in their midgut compared to
147 wild type (Fig 2D-E). These suggest that Iduna promotes Axin degradation *in vivo*.

148 To further understand the contribution of *Iduna* inactivation for both TNKS and Axin
149 proteolysis in *Drosophila*, UAS-Flag-TNKS and UAS-GFP-Axin transgenes were mis-
150 expressed under an eye-specific driver, *GMR*, in an *Iduna* mutant background (Fig
151 S2A). To detect mis-expressed GFP-Axin and flag-Tankyrase levels, total proteins were
152 extracted from five day-old male heads and analyzed by immunoblotting (Fig S2C and
153 E). We found that *Iduna* mutants had 2.5-fold more mis-expressed GFP-Axin protein
154 when compared to the control (Fig S2D). These mutants had 3.5-fold more ectopic
155 expressed flag-tagged Tankyrase as well (Fig S2F). When we examined the eye
156 morphology, GFP-Axin mis-expression did not cause obvious eye phenotype (Fig S2A).

157 On the other hand, mis-expressed flag-tagged Tankyrase led to rough eyes. This
158 phenotype was more severe when *Tnks* was mis-expressed in *Iduna*$^{-/-}$ homozygous
159 mutants compared to *Iduna*$^{-/+}$ heterozygous animals. (Fig S2B). Recently, it was also
160 reported that mis-expressed Tankyrase promotes apoptosis in the *Drosophila* eye due
161 to the activation of JNK signaling (Feng et al., 2018).

162 In order to examine whether Axin is a target for Iduna-mediated degradation, we also
163 mis-expressed a UAS-GFP-Axin transgene under the enterocyte specific temperature
164 sensitive *Myo1A-Gal4* driver (Fig S3A) and saw 2-2.5 fold more Axin in *Iduna* mutants
165 compared to controls (Fig S4B). To investigate the cellular levels of Myo1A driven GFP-
166 Axin in the enterocyes, we examined *FRT80B, Iduna* mutant clones and found that
167 mutant enterocyte clones had more GFP-Axin when compared to their neighboring cells
168 (Fig S4C). Taken together, these observations suggest that Iduna plays a role in
169 promoting the degradation of both Axin and TNKS.

170 **Iduna is required to control the proliferation of intestinal progenitors in the**
171 ***Drosophila* midgut:** Attenuations in the Wingless pathway cause over-proliferation of
172 stem cells in the *Drosophila* midgut. For instance, inactivation of *Tcf*, *arr, armadillo, dsh,*
173 and *pygo* leads to suppression of Wingless signaling, which in turn causes more stem
174 cell division (Kramp et al., 2002; Wang et al., 2016a and 2016b; Tian et al., 2016). On
175 the other hand, *Apc* and *Tnks* mutations cause elevation of Axin, reduce wingless
176 signaling and mitosis of stem cells in *Drosophila* (Wang et al., 2016a and 2016b; Tian et
177 al., 2016). Hence, the Wingless signaling pathway is required to control intestinal stem
178 cell proliferation in *Drosophila* (Xu et al, 2011; Cordero et al., 2012; Tian et al., 2016).

179 Since *Iduna* mutants have elevated Axin level, we considered that *Iduna* inactivation
180 may cause aberrant proliferation of stem cells in the *Drosophila* midgut. Just as the
181 mammalian intestine (Korinek et al., 1998), the *Drosophila* midgut has intestinal stem
182 cells (ISCs) which give rise to all intestinal compartments (Micchelli et al., 2005;
183 Ohlstein et al., 2005). ISCs give rise to two types of daughter progenitor cells:
184 undifferentiated enteroblasts (EBs) and pre-enteroendocrine cells (Pre-EE). EBs and
185 pre-EEs differentiate into enterocytes (ECs) and enteroendocrine (EEs) cells,
186 respectively (Ohlstein et al., 2005; Xu et al., 2011) (Fig S4A). Stem cells can be
187 distinguished from enterocytes by their cell size and marker proteins (Ohlstein and
188 Spadling 2006; Xu et al., 2011). Stem cells are small, express cell membrane-
189 associated Armadillo, and lack of nuclear Prospero (Fig S4B). In contrast, nuclear
190 Prospero staining is a marker of small-sized differentiated enteroendocrines (Fig S4B).

191 ISCs are also marked by the expression of *escargot (esg),* a transcription factor whose
192 GFP reporter allows tracing of stem and progenitor cells during development (Ohlstein
193 et al., 2005) (Fig S4B). Using the *esg>GFP* marker, we first analyzed 9 day-old female
194 flies which were fed with a 5% sucrose diet for seven days at $28^{O}C$ and saw an
195 approximately twofold increase in the numbers of escargot positive ISCs/progenitors in
196 the midgut of *Iduna* mutants compared to controls (Fig 3A-B). *Iduna* inactivation
197 increased the numbers of $Arm^{+}/Pros^{-}$ stem cells in the midguts (Fig 3C) upon nutrient
198 deprivation.

199 To test whether the increased number of ISCs was dependent on nutrient deprivation,
200 we examined midguts of seven-day old female mutants and controls on regular diet. We
201 saw again an approximately twofold increase in the numbers of both *escargot*>GFP

202 positive (Fig 3D-E) and $Arm^+/Pros^-$ stained (Fig 3F-G) stem cells-progenitors under
203 these conditions. Therefore, increased ISC numbers in *Iduna* mutants are independent
204 of diet.

205 To exclude the possibility that *Iduna* mutant flies raised on regular diet had reduced
206 nutrient uptake, we monitored fly feeding by an acid blue 9 colorimetric assay (Mattila et
207 al., 2018). We noticed no decrease in food intake in *Iduna* mutants kept on regular diet
208 at 24-25°C compared to controls (Fig S1E). These results show that *Iduna* inactivation
209 promotes the numbers of midgut stem cells independent of diet and food intake. Finally,
210 we analyzed the midgut cell composition in *Iduna* mutant and control flies. We
211 observed a slight increase in the total midgut cell number of *Iduna* mutants (Fig S4C).
212 However, there were no significant differences in the number of EC and EE cells (Fig
213 S4D-E). Collectively, these observations indicate that *Iduna* inactivation selectively
214 affects ISC numbers.

215 The observed increase in stem cell numbers could be the result of aberrant stem cell
216 proliferation or inhibition of their differentiation. To distinguish between these
217 possibilities, we first assessed cell proliferation by dissecting 7 day-old mutant or wild
218 type females. Following an hour EdU-labeling of the dissected midguts, we observed
219 that *Iduna* mutants had more EdU-positive cells (Fig 4A-C). Moreover, phospho-Ser-
220 Histone H3 (pH3) immunostaining (Fig 4D-E) also revealed a significant increase in
221 $pH3^+$ mitotic cells in the midgut of seven-day old female *Iduna* mutants (Fig 4D-F).
222 These findings suggest that stem cells undergo increased proliferation in the midgut of
223 *Iduna* mutants. To address whether there was an inhibition of differentiation in *Iduna*
224 mutants, we generated *FRT80B, Iduna* mutant clones (Theodosiou et al., 1998). We

225 found that ECs and EEs were present in the five-day old female mutant clones,
226 demonstrating that Iduna was not essential for differentiation of ISCs into daughter cells
227 (Fig S4F-G).

228 **Regulation of Axin proteolysis by Iduna is necessary for normal ISC proliferation:**
229 One possible mechanism by which Iduna may control the proliferation of ISCs in the
230 *Drosophila* midgut is through modulating the concentration of Axin. To determine
231 whether a reduction of the elevated Axin levels could reduce ISC numbers in *Iduna*
232 mutants, they were recombined with *Axin* mutants and then crossed again with *Iduna*
233 mutants to generate flies that were homozygous mutant for *Iduna*$^{-/-}$ and heterozygous
234 for *Axin*$^{+/-}$. Strikingly, a reduction of the *Axin* gene dosage by 50% restored ISC
235 numbers to wild type levels in *Iduna* mutants (Fig 5A). Compared to seven day-old
236 female controls, *Iduna* mutants had an approximately twofold increase in the number of
237 Arm^{+}/Pros^{-} as well as pH3^{+} mitotic stem cells (Fig 5B-C). On the other hand, reducing
238 the *Axin* gene dosage by 50% in an *Iduna*-Null background yielded numbers of ISCs
239 and the pH3^{+} stem cells comparable to seven day-old wild type females. These results
240 suggest that small changes in the levels of Axin have profound effects on stem cell
241 number, and that regulation of Axin degradation by Iduna is necessary for normal ISC
242 proliferation.

243 We observed that *Iduna* mutants had 2-fold more Axin in the *Drosophila* midgut. This
244 indicates that defects in Axin degradation may cause over-proliferation of stem cells due
245 to inhibition of wingless signaling. Therefore, we analyzed a reporter for the Wingless
246 pathway target gene, *frizzled-3* (*fz3*). It was previously reported that *fz3-RFP* reporter
247 activity is high at the major boundaries between compartments (Buchon et al., 2013;

248 Tian et al., 2016; Wang et al., 2016a, b). *Fz3-RFP* was strongly expressed in
249 enterocytes at three distinct sites of the midgut: around R1a, R2c, and R5 (Buchon et
250 al., 2013). Therefore, enterocytes are the primary sites of the Wingless pathway
251 activation during intestinal homeostasis (Tian et al., 2016).

252 We analyzed 3 day-old *fz3-Gal4>GFP* expressing females and consistently observed
253 that *fz3>GFP* was expressed in gradients in the foregut, posterior midgut, as well as the
254 border between the posterior midgut and hindgut (Fig 5D). Here, we focused on the
255 posterior midgut-hindgut border to investigate the effect of Iduna on wingless signaling.
256 Upon *fz3-Gal4* driven RNAi-mediated *Iduna* depletion, we found that *fz3>GFP* activity
257 decreased significantly (Fig 5E). We conclude that Iduna stimulates *wingless* activity in
258 the posterior midgut by promoting degradation of Axin.

259 The proliferation of stem cells in the *Drosophila* midgut is regulated by intrinsic signals
260 and also interactions with neighboring cells (Zhou et al., 2013; Tian et al., 2016). To
261 further investigate whether the observed effects could reflect a cell-autonomous
262 requirement of Iduna in stem cells, or alternatively a requirement in other cells of the
263 midgut, *Iduna* was specifically targeted in enterocytes as well as midgut stem and
264 progenitors cells by using the *Myo1A-Gal4* and *esg-Gal4* drivers, respectively (Fig 6A-
265 B). We examined 7 day-old females expressing *Iduna* RNAi under the *Myo1A* or *esg*
266 drivers. RNAi-mediated knock-down of *Iduna* in enterocytes caused a significant
267 increase in $Arm^{+}/Pros^{-}$ stem cell numbers (Fig 6B). However, stem cell/progenitor cell-
268 specific knock-down of *Iduna* did not affect either the stem cell numbers or mitosis in the
269 midgut (Fig 6B-C). This suggests that *Iduna* inactivation causes stem cell over-
270 proliferation by a non cell-autonomous mechanism, and that perhaps enterocytes are

271 responsible for stem cell over-proliferation in *Iduna* mutants. To further test this idea,
272 we ectopically expressed *Iduna* in enterocytes and investigated if this could suppress
273 stem cell proliferation in *Iduna* mutants (Fig 6D). Indeed, consistent with this model, we
274 saw that *Myo1A-Gal4* driven UAS-Iduna was able to restore normal numbers of stem
275 cells and progenitors (Fig 6E-F). Taken together, our results indicate that Iduna plays a
276 physiological role to regulate *wingless* signaling in enterocytes, which is critical for
277 proper ISC proliferation.

278 We found that *Iduna* mutants have increased mortality upon nutrient deprivation (Fig.
279 1C). Following 7 days on a 5% sucrose diet at 28°C, *Iduna* mutants had more *esg>GFP*
280 positive cells in the midgut (Fig 3A-C). Therefore, we considered that under reduced
281 nutrient diet, hyper-proliferation of midgut stem cells may be responsible for elevated
282 mortality. To test this idea we first inactivated *Iduna* in enterocytes by expression of
283 three different RNAi lines under the Myo1A driver. We found that RNAi-mediated *Iduna*
284 depletion did not increase lethality compared with *white* RNAi (Fig S5A). There was also
285 no significant change on the mean lifespan between *white* and *Iduna* RNAi expressing
286 flies (Fig S5B). We also tested enteroblast specific *Iduna* depletion and again found no
287 significant effects on longevity upon nutrient deprivation (Fig S5C). Finally, we
288 expressed UAS-*Iduna* transgene *under Myo1A driver* in enterocytes to rescue the
289 elevated mortality in *the* mutants. Whereas the *Iduna* transgene rescued the hyper-
290 proliferation phenotype (Fig S5E), it failed to rescue the mortality of mutants on 5%
291 sucrose diet (Fig S5D). These findings suggest that Iduna mortality is not caused by
292 dysregulation of midgut stem cell proliferation and point to another role of *Iduna* in
293 promoting survival under stress conditions.

294

295 **Depletion of *Iduna* promotes stem cell proliferation through the JAK-STAT**
296 **pathway**: In order to further investigate the mechanism by which Iduna affected ISC
297 proliferation, we explored the function of additional signaling pathways implicated in this
298 system. Because the JAK-STAT pathway has a well-known role in stem cell
299 proliferation (Zeidler et al., 2000; Zoranovic et al., 2013; Zhou et al., 2013; Markstein et
300 al., 2013), we looked for possible effects of *Iduna* mutants here. We analyzed the JAK-
301 STAT pathway via 10x Stat-GFP reporter line in the midgut (Bach et al., 2007).
302 Under regular physiological conditions, Stat-GFP reporter expression was mainly seen
303 in small sized cell populations in the midgut that appear to represent ISCs for several
304 reasons (Fig S6). First, Prospero-positive enteroendocrine cells were negative for Stat-
305 GFP (Fig S6A). Second, enterocytes stained with Armadillo were also not expressing
306 the Stat-GFP reporter (Fig S6D). Finally, Delta-lacZ positive but Prospero-negative cells
307 for the most part expressed Stat-GFP. However, a minor population of small sized cells
308 was GFP positive but Delta-lacZ negative (white arrows, Fig S6B). These appear to be
309 undifferentiated progenitors, such as enteroblasts. Seven day-old *Iduna* mutants had
310 more Stat-GFP positive cells when compared to controls (Fig 7A, S7A-F). We also
311 generated *FRT80B, Iduna* midgut mutant clones and observed that these clones had
312 elevated JAK-STAT signaling (Fig S7A-B). To confirm elevated JAK-STAT signaling in
313 *Iduna* mutant stem cells, we stained midguts from seven day-old females for Delta, a
314 previously identified JAK-STAT pathway target gene (Jiang et al., 2009). We found that
315 there was indeed more Delta protein in *Iduna* mutants, consistent with elevated JAK-
316 STAT activity (Fig S7G).

317

318 To test whether activation of JAK-STAT signaling was responsible for aberrant ISC
319 proliferation, we knocked down *stat92E*, a transcription factor in the JAK-STAT
320 pathway, in enterocytes as well as in stem cells and progenitors. We did not detect
321 dramatic changes in the numbers of mitotic cells when *stat92* transcription factor was
322 depleted in enterocytes (Fig 7B). Interestingly, knock-down of *stat92E* in midgut stem
323 and progenitors cells was sufficient to suppress their increased cell division (Fig 7B).
324 Collectively, these observations suggest that *Iduna* inactivation causes decrease in
325 *wingless* signaling in enterocytes which in turn causes elevated JAK-STAT signaling in
326 midgut stem cells and thereby results in their over-proliferation.

327

328 Our observations raise the question of how enterocytes signal ISC proliferation. One
329 possibility is that enterocytes secrete a factor activating the JAK-STAT pathway in stem
330 cells. The JAK-STAT pathway can be activated by cytokines, such as *unpaired* (UPD,
331 UPD2, UPD3) in the *Drosophila* midgut (Ghiglione et al., 2002; Zhou et al., 2013). Upd3
332 is produced in differentiated ECs and in differentiating enteroblasts (Zhou et al., 2013).
333 Therefore, we explored the possibility that *unpaired* cytokines could mediate stem cell
334 over-proliferation in *Iduna* mutants. For this purpose, we first inactivated *Iduna* with the
335 *Upd3-Gal4* driver and found that RNAi-mediated knock-down of *Iduna* resulted in a
336 significant increase of *Upd3>GFP* reporter expression in the midgut (Fig 7C-D, Fig
337 S8A). *Upd3>GFP*-positive cells were mainly enterocytes, and not EEs or ISCs (Fig 7E,
338 Fig S8B-C). We then knocked down *Iduna* in enterocytes and performed a q-PCR to
339 test whether *Iduna* depletion in enterocytes induced unpaired expression. We detected

340 that enterocyte specific *Iduna* inactivation resulted in elevated *Upd3* gene expression
341 compared to *white* RNAi (Fig 7D). To suppress the over-proliferation of midgut stem cell
342 in *Iduna* mutants, we finally reduced *Upd2* and *Upd3* gene dosages. Strikingly, we
343 found that heterozygosity in Δ*Upd2-Upd3* fully suppressed ISC proliferation in *Iduna*
344 mutants (Fig. 7E). Secreted Unpaired proteins bind to the Domeless receptor on ISCs
345 (Ghiglione et al., 2002). Therefore, we tested whether decreasing Domeless levels
346 could also suppress stem cell over-proliferation in *Iduna* mutants. Again, this prediction
347 was experimentally confirmed (Fig 7E). We conclude that inactivation of *Iduna* causes
348 decrease in wingless signaling in enterocytes, which in turn leads to increased secretion
349 of UPD2-3 from these cells to stimulate over-proliferation of ISCs through the JAK/STAT
350 pathway (Fig 7F).
351

352 **Discussion**

353 In this study, we investigated the *in vivo* function of *Iduna* and identified a critical role of
354 this enzyme for the control of stem cell proliferation in the *Drosophila* midgut. It was
355 previously shown that mammalian Iduna is an unusual E3-ubiquitin ligase that
356 specifically binds to and poly-ubiquitylates ADP-ribosylated substrates to promote their
357 rapid degradation by the proteasome. However, the physiological function of Iduna
358 remains largely unclear. Here, we generated *Drosophila* Null-mutants and used them to
359 show that Iduna has an important *in vivo* function for the degradation of ADP-ribosylated
360 TNKS and Axin to control stem cell proliferation. In particular, we focused on the role of
361 *Iduna* in the *Drosophila* midgut. We found that *Iduna* inactivation caused a slight but
362 significant increase in Axin protein levels in enterocytes, which in turn caused over-

363 proliferation of intestinal stem cells. This non-cell autonomous effect on stem cell
364 proliferation was depended on UPD2-UPD3 cytokines that are secreted from
365 enterocytes. These findings suggest a model in which loss of Iduna function, which
366 decreases the Wingless pathway activity due to elevated Axin levels in enterocytes,
367 which in turn causes increased secretion of UPD2-3 resulted from these cells to activate
368 the JAK-STAT pathway in ISCs. Importantly, a 50% reduction in *Axin* gene dosage
369 blocked the over-proliferation of stem cells in *Iduna* mutants, demonstrating the
370 necessity to tightly regulated Axin levels in this system. Whereas many other cell types
371 appear to tolerate fluctuations in the amount of Axin protein, proper wingless signaling
372 in the *Drosophila* midgut appears to critically depend on restricting Axin levels by Iduna.
373 The activity of Iduna depends on binding to ADP-ribosylated substrates via its WWE
374 domain. Recognition and binding to its ADP-ribosylated target proteins change the
375 structural confirmation of Iduna. Subsequently, Iduna is activated to ubiquitylate its
376 targets for proteasome-mediated degradation. It was previously reported that TNKS
377 forms a tight complex with Iduna to control the proteolysis of target proteins (DaRosa et
378 al., 2015). We could not detect any obvious morphological differences between *Iduna*
379 mutants and wild type. Although this may seem somewhat surprising, it is consistent
380 with inactivation of *Tnks* in *Drosophila,* which also causes no overt abnormalities (Feng
381 et al., 2014; Wang et al., 2016a and 2016b; Yang et al., 2016). Like for *Iduna*, *Tnks*
382 mutants have no obvious effects on wing development and the expression of *wingless*
383 target genes in larval wing discs, despite the fact that Axin levels are increased (Feng et
384 al., 2014; Wang et al., 2016a and 2016b; Yang et al., 2016). Our interpretation of these
385 findings is that most tissues can tolerate relative modest (2-3-fold) changes of Axin. For

386 example, it appears that a greater than 3-fold increase of endogenous Axin is required
387 for functional consequences of altered wingless signaling in *Drosophila* embryos (Yang
388 et al., 2016) and 3-9-fold changes are needed in wing discs (Wang et al., 2016a). On
389 the other hand, the *Drosophila* midgut appears much more sensitive to reduced
390 Wingless signaling.
391 A recent study demonstrated that inactivation of *Drosophila Tankyrase (Tnks)* also led
392 to increased Axin protein accumulation in the *Drosophila* midgut and promoted ISC
393 proliferation as well (Wang et al., 2016). These results are consistent with previously
394 reported cell-based studies suggesting that Iduna mediates Tankyrase-dependent
395 degradation of Axin and thereby positively regulates Wnt signaling (Huang et al., 2009;
396 Zhou et al., 2011; Croy et al., 2016; Callow et al., 2011). On the other hand, it is
397 somewhat surprising that inactivation of two highly diverse types of enzymes,
398 *Tankyrase*, a poly-ADP-ribose polymerase versus *Iduna*, a ubiquitin E3 ligase, produces
399 remarkably similar phenotypes. Both Tnks and Iduna have many other targets outside
400 the Wnt-pathway, and based on biochemical observations it has been proposed that
401 they may play roles in DNA repair, telomere length, vesicle trafficking, Notch-signaling,
402 centrosome maturation, neuronal protection and cell death (Bai et al., 2012; Gibson et
403 al., 2012; Riffel et al., 2012). However, *Iduna* mutant flies are viable and do not show
404 any obvious defects under normal growth conditions. This indicates that the major non-
405 redundant physiological function of both Tnks and Iduna in *Drosophila* is to regulate
406 Wingless-mediated intestinal stem cell proliferation, and that it provides physiological
407 evidence for the idea that the function of both proteins is indeed tightly coupled. In
408 addition, our study identifies a role of Upd/Dome in this pathway. These results may

409 also have implications for the regulation of this highly conserved pathway in mammals.
410 For example, conditional inactivation of *Iduna* in mouse bones leads to increased
411 numbers of osteoclasts and inflammation (Matsumoto et al., 2017a). In this system,
412 down-regulation of *Iduna* leads to accumulation of Axin1 and 3BP2. This, in turn,
413 attenuates β-catenin degradation and activates SRC kinase, respectively, thereby
414 promoting the release of inflammatory cytokines in the bone (Matsumoto et al., 2017a).
415 On the other hand, *Iduna* depletion reduces proliferation of osteoblasts and promotes
416 adipogenesis in the mouse skeleton (Matsumoto et al., 2017b). Despite the obvious
417 differences between mammalian bone and the *Drosophila* midgut, both systems show
418 overall striking similarities in the use of TNKS/Iduna to restrict Axin levels to achieve
419 proper levels of Wnt/β-catenin signaling during tissue homeostasis. Finally, our study
420 also indicates that Axin may have a more general function as a scaffold protein to
421 recruit multiple proteins to permit a crosstalk with other pathways to modulate Wnt/β-
422 catenin signaling.
423

424 **Figure Legends**

425 **Figure 1: Loss-of-function mutants of *dIduna* are viable and increase TNKS and**
426 **Axin protein levels. A-** *Iduna*^{17} and *Iduna*^{78} have deletions of 4 and 2 nucleotides,
427 respectively, introduced early stop codons and led to truncations of Iduna protein.
428 Scheme for generation of *Iduna* loss-of-function mutants via CRISPR-Cas9 genome
429 editing in *Drosophila.* sgRNA against Iduna was designed to generate small nucleotide
430 deletions, close to its translation initiation site. The three nucleotides were highlighted
431 with red to indicate the location of Cas9 cleavage site. *Iduna* loss-of-function mutants,
432 *Iduna*^{17} and *Iduna*^{78}, were isolated by Sanger sequencing**. B-** *Iduna*^{17} and *Iduna*^{78} have
433 no detectable protein. Endogenous Iduna protein was detected by immunoblotting. Anti-
434 Iduna antibody was generated in guinea pigs and 20μg total protein lysates of seven
435 day-old adult females were analyzed by immunoblotting. β-actin was used as a loading
436 control. Both *Iduna* alleles have no detectable protein and behave genetically as Null-
437 alleles. **C-** *Iduna* mutants display increased mortality under reduced nutrient conditions.
438 Two-day old mutant or wild type female flies were collected and kept on 5% sucrose
439 diet at 28°C. n=100 from each genotype. **D**- There is an approximately twofold increase
440 in the numbers of *esg>GFP* expressing stem cells/progenitors in the midgut of *Iduna*
441 mutants compared to controls. **E-** Quantification of *esg>GFP* positive stem cells and
442 progenitors from adult flies of indicated genotypes. n=6 from each genotype. **F**- *Iduna*
443 inactivation increases the numbers of Arm^{+}/Pros^{-} stem cells in the midguts upon nutrient
444 deprivation. Nine day-old female flies, fed with 5% sucrose diet for seven days at 28°C,
445 were examined in D-E and F. Posterior midguts were analyzed in this study. *p<0.001* is
446 indicated as ***.

447 **Figure 2: *Iduna* inactivation causes increased Axin protein levels in the midgut.**
448 **A-** *Iduna* mutant midguts have elevated Axin protein. Midguts of 7 day-old adult females
449 expressing GFP-Axin under the temperature sensitive *Myo1A-Gal4* driver were
450 dissected, lysed and analyzed by GFP immunoblotting. *Iduna* mutants had more Axin
451 protein compared to the wild type. 20μg total intestinal lysates were analyzed by GFP
452 immunoblotting and α-tubulin was used as a loading control. **B-** Loss-of-*Iduna* resulted
453 in 2.2-fold GFP-Axin accumulation in the midgut. Western blot quantification was
454 performed based on two independent experimental replicates, and protein levels were
455 normalized to α-tubulin. **C-** Iduna recognizes ADP-ribosylated (ADPR) Axin via the R252
456 residue of its WWE domain. This residue corresponds to R163 in the mammalian Iduna
457 ortholog and is conserved during evolution. Recombinant wild type and R252A mutants
458 were used as biochemical sensors to pull down the ADPR-Axin from *Drosophila*
459 midguts. Myc-tagged WWE proteins were expressed and purified from *Drosophila* S2R+
460 cells by immunoprecipitation. **D-** Inactivation of *Iduna* leads to accumulation of ADPR-
461 Axin. Wild type myc-tagged-WWE protein pulled down ADPR-Axin. In contrast, the
462 R252A mutant did not interact with modified Axin. Following IP, eluted proteins were
463 analyzed with an α-PAR antibody. The 50kDa heavy chain IgG is indicated on the blot.
464 **E-** *Iduna* inactivation results in 2.3-fold more ADPR-Axin protein in the midgut. Western
465 blot quantification of two independent experimental replicates; ADPR-Axin levels were
466 normalized to the control lines. Flies were fed with regular diet at 24-25°C. $p<0.001$ is
467 indicated as *** and $p<0.0001$ was marked as ****.

468 **Figure 3: *Iduna* mutants have increased numbers of intestinal stem and**
469 **progenitor cells in their midgut. A-B-** Inactivation of *Iduna* promotes the proliferation

470 of the esg-GFP labeled progenitor cells in the *Drosophila* midgut. Intestinal stem and
471 progenitor cells were visualized with a *esg>GFP* reporter construct. **C-** Quantification of
472 *esg>GFP*$^{+}$ stem cells and progenitors from adult flies of indicated genotypes. **D-** In wild
473 type, 25-30% of posterior midgut cells are stem cells, as assessed by *esg>GFP*
474 expression. On the other hand, 55-60% of the total cell population in *Iduna* mutants
475 expressed the stem marker *esg>GFP*, representing a greater than two-fold increase. **E-**
476 **F-** *Iduna* mutants have more Arm^{+}/Pros^{-} intestinal stem cells in the midgut. ISCs and
477 enterocytes were distinguished by their cell size, high level of membrane-associated
478 Armadillo, and lack of nuclear Prospero staining. In contrast, small-sized differentiated
479 enteroendocrines were recognized by nuclear Prospero staining. Posterior midguts
480 were analyzed by confocal microscopy following staining for anti-Armadillo, Prospero
481 and DAPI. **G-H** Quantification of Arm^{+}/Pros^{-} ISCs from adult flies of indicated genotypes.
482 The midguts of seven day-old adult females were dissected and analyzed by confocal
483 microscopy. For the consistency, posterior midgut R5 region was analyzed in this study.
484 *Iduna*$^{17/+}$ flies were used as control. Flies were fed with regular diet at 24-25°C. n>12
485 from each genotype. *p<0.001* was indicated as *** and *p<0.0001* was marked as ****.

486 **Figure 4: *Iduna* inactivation enhances proliferation of intestinal stem cells. A-B-**
487 Genetic depletion of *Iduna* leads to over-proliferation of intestinal stem cells in the
488 midgut. EdU was used as a proliferation marker and administrated for 1h at 25^{0}C. 7
489 day-old mutants or wild type female flies were dissected for analysis. Following fixation,
490 EdU incorporation was analyzed by confocal microscopy. **C-** Increased numbers of
491 EdU^{+} stem cells were seen in *Iduna* mutants, indicating increased cell proliferation.
492 Posterior midguts were analyzed for quantification. **D-E-** *Iduna* mutants display elevated

493 phospho-Ser-Histone 3 (pH3)-positive ISCs**. F-** Iduna inactivation leads to an increase
494 of $pH3^+$ mitotic stem cells in the midgut. Quantification of $pH3^+$ proliferating cells was
495 done in the whole midgut. 7 day-old mutants or wild type female flies were examined.
496 Flies were fed with regular diet at 24-25°C. n>12 from each genotype. *p<0.0001* was
497 marked as ****.

498 **Figure 5: A 50% reduction of *Axin* restores ISC numbers in the *Drosophila***
499 **midgut. A-** Reducing the *Axin* gene dosage by half restores the number of $Arm^+/Pros^-$
500 ISCs. *Axin* mutants *AxinS044230* and *AxnE77* were recombined with the $Iduna^{17}$ mutant
501 allele. *AxinS044230* is a complete *Axin*-Null mutant, and *AxinE77* is a loss-of-function
502 truncation allele (Q406X). Midguts of 7d-old adult females of the indicated genotypes
503 were dissected and analyzed by confocal microscopy following Armadillo, Prospero and
504 DAPI staining. $Axin^{+/-}$, $Iduna^{17/+}$ served as control. Reducing the Axin gene dosage by
505 50% in $Iduna^{17/17}$ mutants decreased the number of ISCs to normal levels. **B-**
506 Quantification of ISC numbers. Reducing the *Axin* gene dosage by half fully suppressed
507 the increased numbers of $Arm^+/Pros^-$ ISCs in $Iduna^{17/17}$ Null-mutants. **C-** Reducing *Axin*
508 gene expression suppressed the proliferation of ISCs in the $Iduna^{17/17}$ Null-mutant.
509 *p<0.0001* was marked as ****. **D-** *Frizzled 3 (fz3)* is a *wingless* target gene and a GFP-
510 reporter construct was used here to visualize Wg-activity in the midgut (Buchon et al.,
511 2013; Tian et al., 2016; Wang et al., 2016a, b). In wild type, *fz3>GFP* is highly
512 expressed in a graded fashion in the foregut (f), the posterior midgut (p) as well as the
513 posterior midgut-hindgut border, but not in the anterior midgut (a) or the hindgut proper
514 (h). Higher magnification image of the *fz3>GFP* near the midgut-hindgut boundary. 7-
515 day old female midguts were analyzed. **E-** *fz3-Gal4* driven *Iduna* depletion inhibits

516 *wingless* activity. RNAi-mediated down-regulation of *Iduna* led to significant reduction of
517 *fz3>GFP*; *white RNAi* served as a control. The arrow indicates the border between the
518 posterior midgut and the hindgut (b). Three day-old female midguts were analyzed.
519 Flies were fed with regular diet at 24-25°C.

520 **Figure 6: *Iduna* depletion in ECs leads to over-proliferation of ISC. A-** Over-
521 proliferation of ISCs in *Iduna* mutants is non-cell autonomous. RNAi-mediated *Iduna*
522 knock-down was carried out in the enterocytes, stem cells and enteroblast cells using
523 *Myo1A-Gal4* and *esg-Gal4* drivers, respectively. **B-** Knock-down of *Iduna* in enterocytes
524 using the *Myo1A-Gal4* driver led to over-proliferation of Arm^{+}/Pros^{-} ISCs. In contrast, no
525 changes in ISC proliferation were observed upon down-regulation of *Iduna* in ISCs
526 using *esg-Gal4*-driven *Iduna* RNAi. *Myo1A-Gal4*>GFP served as a control. **C-** EC-
527 specific knock-down of *Iduna* increased the number of pH3^{+} progenitors. **D-** Ectopic
528 expression of *Iduna* in ECs inhibits over-proliferation of ISCs. A UAS-Myc-tagged Iduna
529 C/G transgene was generated to perform rescue experiments. **E- F-** Expression of the
530 UAS-Myc-Iduna C/G transgene with the *Myo1A-Gal4* driver resulted in a reduction of
531 the numbers of Arm^{+}/Pros^{-} ISCs and pH3^{+} mitotic stem cells in the midgut of *Iduna*
532 mutants. Flies were fed with regular diet at 24-25°C. 7 day-old female midguts were
533 analyzed for ISC and mitotic markers. *p<0.0001* was marked as ****.

534 **Figure 7: Loss of *Iduna* activates the JAK-STAT pathway non-cell autonomously**
535 **to promote ISC proliferation. A**- *Iduna* mutants have elevated Stat-GFP signaling in
536 ISCs. *10X-Stat-GFP* is a reporter for STAT signaling activity. *Iduna* mutants displayed
537 strongly increased GFP reporter. 7 day-old females were dissected and the posterior
538 midguts were analyzed. **B-** Quantification of Stat-GFP expressing midgut cells. **C-**

539 Knock-down of the *stat93E* transcription factor in ISCs and EBs blocks ISC over-
540 proliferation in *Iduna* mutants. In contrast, RNAi-mediated depletion of *stat92E* in ECs
541 did not affect proliferation of ISCs. 7 day-old female midguts were dissected and
542 analyzed. **D-** *Iduna* depletion results in upregulation of *Upd3* mRNA expression in
543 enterocytes. Myo1A driven *Iduna-RNAi* and *white RNAi* expressing 7 day-old females
544 were dissected for their midguts. Total RNA was isolated and cDNA libraries were
545 prepared. *Upd3* transcripts were amplified and analyzed by q-PCR. **E**- RNAi-mediated
546 *Iduna* down-regulation induces *Upd3>GFP* reporter activity. *Iduna* was knocked-down
547 using RNAi driven by *Upd3-Gal4*, and *GFP* was used as a reporter for *Upd3* gene
548 expression. Enterocytes were stained with α–Armadillo antibody. EEs and ISCs were
549 negative for Upd3>GFP expression. *white RNAi* served as a control. 3 day-old female
550 flies were dissected and their posterior midguts were analyzed by confocal microscopy.
551 **E-** Reduction of either *Upd2 and Upd3* or their receptor *Domeless* suppresses over-
552 proliferation of ISCs in *Iduna* mutants. Upon reduction of *Upd2* and *Upd3* gene dosage
553 in *Iduna* mutants, we observed significantly less mitotic stem cells in *Iduna* mutants,
554 comparable to WT levels. Likewise, a 50% reduction of *Domeless* resulted in
555 suppression of ISC over-proliferation in *Iduna* mutants. On the other hand, these
556 reductions in gene dosage of *Upd2, Upd3* and *Dome* did not affect mitosis of ISCs in a
557 WT background. 7 day-old female midguts were quantified by $pH3^+$ staining. Flies were
558 fed with regular diet at 24-25°C. n>12 from each genotype. *p<0.0001* was marked as
559 ****. **G-** Model for the role of *Iduna* in the regulation of intestinal stem cell proliferation.
560 Our model suggests that inactivation of *Iduna* causes Axin elevation which in turn
561 decreases wingless signaling activation in enterocytes, and increases secretion of UPD

562 cytokines from these cells. These cytokines activate JAK-STAT signaling through the
563 Dome receptor on neighboring ISCs and thereby induce ISC proliferation in the
564 *Drosophila* midgut.

565

566 **Material and Methods**

567 **Fly stocks:** Flies were kept at a 12-hour light/dark cycle. All crosses were performed at
568 22-25°C unless stated otherwise. The following fly stocks were used for this study
569 (Bloomington Drosophila Stock Center (BDSC) and Vienna Drosophila Resource Center
570 (VDRC) number (#) given in parentheses):
571 The stocks used in here: Df(3L)Exel6135 (BDSC# 7614), Df(3L)ED228 (BDSC#
572 8086), Df(3L)ED229 (BDSC# 8087), esg-Gal4, UAS-GFP (a gift of Dr. Norbert
573 Perrimon, Micchelli et al., 2006), esgK606 (a gift of Dr. Norbert Perrimon, Micchelli et
574 al., 2006), *10X STAT-GFP*, Bach et al., 2007), UAS-GFP-Axin (BDSC# 7224), FRT82B,
575 *Axin044230* (a gift of Dr. Wei Du, Hamada et al., 1999), FRT82B, *AxinE77* (a gift of Dr.
576 Jessica Treisman, Collins et al., 2000), Myo1A-Gal4, tub-Gal80ts, UAS-GFP (a gift of
577 Dr. Norbert Perrimon, Micchelli et al., 2006), Upd3-Gal4, UAS-GFP (a gift of Dr. Norbert
578 Perrimon, Markstein et al., 2013), ∆Upd2/3 (BDSC# 129), ∆Dome (BDSC# 12030),
579 UAS-*stat92E* RNAi (BDSC# 26889), UAS-CG8786/*dIduna* RNAi#1 (BDSC# 40882),
580 UAS-CG8786/*dIduna* RNAi#2 (VDRC#43533), UAS-CG8786/*dIduna* RNAi#3
581 (VDRC#36028), UAS-CG8786/*dIduna* RNAi#4 (VDRC#36029), and *white* RNAi
582 (BDSC#33623), fz3-Gal4 (BDSC#36520). The rest of *Drosophila* lines, which were
583 studied here, were obtained from Steller Lab stocks. Oregon R flies were used as
584 control and only adult female flies were analyzed in this study.
585 ***Drosophila* egg collection:** A 10mm^2 apple-agar plate was set up with embryo
586 collection cage to provide a substrate for egg laying. Prior to adding the plate, a small
587 quantity of yeast paste was smeared onto the center of the apple-agar. To provide
588 moisture, water soaked tissue paper was layered under embryo collection cages. 10-15

589 day old adult flies were collected to the cage, which were then placed into a fly
590 incubator for 4 hours. Then, laden eggs were counted and 50 of them were plated into
591 one corner of 10cm^2 apple-agar plates, in which had a straight yeast paste smear at the
592 center. Agar plates finally were incubated in the incubator. After 24h, hatched eggs
593 were counted.
594 To analyze larval development, hatched 1st instar larvae were counted and placed into a
595 fresh yeast paste containing agar plate until they were reached to 3rd instar larvae. After
596 counting, larvae were placed into regular food containing vials. They were counted two
597 rounds when they pupated and enclosed.
598 **5% sucrose diet:** 5mm^2 Whatman filter papers were soaked with 1ml 5% sucrose
599 solution and placed into the empty vials. 5% sucrose solution was used as reduced
600 nutrient diet. Enclosed adult females were collected at 24-25°C. When they were 2 day-
601 old, their regular diet was replaced to 5% sucrose diet at 28°C. 20 of two day-old wild
602 type or *Iduna* mutant female flies were grouped and kept on 5% sucrose solution-
603 soaked filter paper containing vials at 28°C. Following the fly count, death flies were
604 removed and 1ml 5% sucrose-embedded filter papers were replaced with a new one
605 everyday.
606 **Food intake measurement:** Female flies of *Iduna* mutant and Oregon R were collected
607 after they enclosed. Before measuring food intake, the flies were kept on the regular
608 food for 6 days. The flies then transferred to the regular food supplemented with 0.5%
609 (w/v) Acid Blue 9 (erioglaucine disodium salt, Sigma 861146) for 4 hours.
610 Quandruplicates of 5 flies per sample were then homogenized in 250μl 1xPBS and
611 cellular debris was removed by centrifugation. Food intake was quantified by measuring

612 the absorbance of the supernatant at 630nm and normalized to the wet weight of the
613 flies.

614 ***CG8786/dRNF146/dIduna* CRISPR/Cas9 editing:** We used the CRISPR optimal target
615 finder website (tools.flycrispr.molbio.wisc.edu/targetFinder) to identify an appropriate
616 guide RNA (gRNA) target sequence within *dIduna* (Granz et al., 2013 and 2014). We
617 purchased the forward 5`-GTCGCTAGCTGCAATCTGCTCTG-3` and reverse 5`-
618 AAACCAGAGCAGATTGCAGCTAG-3` oligos (IDT, Inc.) annealed, and followed the
619 protocol; from Port et al., 2014 to clone the annealed oligos into pCFD3-dU6:3-gRNA
620 plasmid (Addgene, plasmid# 49410, Port et al., 2014). Transformants were verified via
621 Sanger sequencing (Genewiz, Inc.). The gRNA plasmid was injected into 300 embryos
622 of custom *vasa*-Cas9 *Drosophila* (BestGene, Inc.). The injection was yielded 89 G_o
623 progeny, and we established 70 individual fly lines, a couple of which could possibly
624 have the *Iduna* loss-of-function mutations.

625 **Isolation of the *Iduna* mutants and genetic mapping of *Iduna* –loss-of-function**
626 **mutations**: Total DNA was isolated from L3 larvae or 5-days old adults of *Iduna*
627 homozygous mutants and control sequencing strain using the Roche genomic DNA
628 extraction kit (Roche). To confirm the mutant line, PCR fragments were amplified with
629 specific primers (forward primer 5`-CAGCCCGAGCTGGTCATACTCAG-3`, reverse
630 primer 5`-CGGCTTTCTGGGCTACCTAC-3`) binding within 5` UTR of *Iduna* and within
631 the coding region of the gene. To identify mutation site, the entire coding region was
632 PCR amplified and PCR products were sent for DNA sequencing.

633 **Cloning and generation of UAS-CG8786 transgenic *Drosophila*:** Adult flies were
634 directly homogenized in 1ml TRIzol (Life Technologies) and total RNA was isolated

635 according to the manufacturer's protocol. cDNA library was prepared from 5 µg total
636 RNA, by using oligo(dT) amplification and the Superscript III First Strand synthesis kit
637 (Invitrogen). cDNA library was used to amplify the *Iduna* transcripts with the primers
638 (forward 5`-ATGTCGCAACAGCGCTCCACAG-3`; *Iduna* B isoform reverse primer 5`-
639 TCAGTAGAGCTTTAGGTATACC-3`; *Iduna* C/G isoform reverse primer 5`-
640 TCAGTAGAGCTTTAGGTATACCG-3`). Amplified *dIduna* transcripts were cloned into
641 pUAST (DGRC, Drosophila Genomic Resource Center) and pAc5.1 (Thermo Scientific)
642 vectors by considering the appropriate restriction digestion sites. Following the bacterial
643 transformation, all of the cloned genes were sequenced. To generate UAS-CG8786
644 transgenic *Drosophila,* myc-tagged pUAST-CG8786/dIduna plasmid was injected into
645 w1118 embryos (Best Gene, Inc.) We obtained successful transgenic lines.
646 **Total RNA isolation, cDNA synthesis and Q-PCR:** Posterior midguts of 7 day-old
647 adult flies were directly homogenized in 1 ml TRIzol (Life Technologies) and total RNA
648 was isolated according to the manufacturer's protocol (miRNeasy mini kit, QIAGEN).
649 cDNA library was prepared from 5 µg total RNA, by using oligo(dT) amplification and the
650 Superscript III First Strand synthesis kit (Invitrogen). cDNA library was used to amplify
651 *Upd3* and *Rp32l* transcripts with the forward 5`-AGGCCATCAACCTGACCAAC-3`,
652 reverse 5`-ACGCTTCTCCATCAGCTTGC-3` and forward 5`-
653 CCCAAGGGTATCGACAACAGA-3`, reverse 5`-CGATCTCGCCGCAGTAAAC-3`
654 primers, respectively. Those primers were designed via the online tool of DRSC/TRiP
655 Functional Genomics Resources, Harvard Medical School and purchased from IDT, Inc.
656

657 **Cloning and generation of the wild type and mutants UAS-Flag-Tnks transgenic**
658 ***Drosophila*:** We previously described *Drosophila* TNKS (Park and Steller, 2013) and its
659 ORF was cloned into pUAST vector from pcDNA3.1-Flag-TNKS. To generate UAS-
660 Flag-TNKS transgenic *Drosophila,* Flag-tagged pUAST-TNKS plasmid was injected into
661 w1118 embryos (Best Gene, Inc.) We obtained successful transgenic *Drosophila* lines
662 and those were utilized in conjunction with tissue-specific *Gal4* drivers.
663 **Clone analysis and RNAi experiments:** Mutant clones were utilized to generate
664 mitotic clones. 2nd instar larvae were subjected to an hour heat shock in a 37^0C water
665 bath per day until they reached the pupa stage and maintained at 24^0C. 3-days old adult
666 females were analyzed.
667 For RNAi experiment, crosses were performed at 24^0C and the progeny of the desired
668 genotypes were collected on the day of eclosion and maintained at 24^0C for 7 days
669 before dissection. In the case of using temperature sensitive driver, eclosed virgin
670 females were collected and kept at 29^0C for 7 days for intestine dissection.
671 **Cell culture**: S2R+ cells were maintained at 25°C in supplemented Grace's Insect
672 Medium (supplemented with 10% heat inactivated FBS, 100U/ml penicillin, 100µg/ml
673 streptomycin) in spinner flasks.
674 **Development of polyclonal antibodies**: Full-length GST-tagged-Iduna C/G protein
675 was expressed and purified from BL21 DE3 *E.coli* strain. Polyclonal antisera were
676 generated in two guinea pigs (Cocalico, Inc.). For Western blot analysis, serum was
677 used in 1:1000 dilutions.
678 **Western blot analysis**: 50-100µg dissected tissues or total larvae/flies were lysed in
679 lysis buffer [50mM HEPES-KOH pH 7.4, 150mM NaCl, 0.05% Triton-X100, complete

680 EDTA-free protease inhibitor cocktail (Roche)] using a 1 ml tissue grinder. Lysates were
681 cleared by centrifugation at 13,000 g for 20 min at 4°C. Protein concentrations of
682 supernatants were determined by BCA assay (Pierce). 1μg/μl lysate was prepared with
683 3X sample buffer in 100μl total volume (200mM Tris-HCl, pH 6.8, 200mM dithiothreitol
684 (DTT), 8% SDS, 24% glycerol, 0.04% bromophenol blue), heated at 95°C for 10 min
685 and samples were separated by SDS-PAGE for 1 h at 120V, by using standard 1X SDS
686 Tris base-glycine running buffer. Proteins on the gels were blotted onto a PVDF
687 membrane, in a 1X transfer buffer (25mM Tris base, 190mM Glycine, 20% MeOH,
688 0.05% SDS), and transferred (Bio-Rad) at 100V for 90 min. Membranes were taken
689 through a standard immunoblot protocol followed by enhanced chemiluminescent
690 detection (Crescendo ECL, Millipore) using a Lumimager (Fuji, LAS-3000). Primary
691 antibodies: α- tubulin (1/1000, Sigma), α-flag (1/1000, Cell Signaling Technologies), α-
692 myc tag (1/1000, Cell Signaling Technologies), GFP (1/2500, Santa Cruz), β-actin
693 (1/1000), α-PAR (1/1000, Trevigen) and α-Axin (Feng et al., 2014; dT20 *Drosophila*
694 Axin antibody, 1/250, Santa Cruz). Secondary antibodies: anti-mouse, anti-rabbit, anti-
695 guinea pig (1/5000, Jackson Labs)**.**
696 **Immunofluorescence:** Adult intestines were dissected in 1xPBS and fixed in 4%
697 paraformaldehyde in PBS for 45 min at room temperature. Tissues then were first
698 washed with 0.1% Tween 20-PBS, second washed with 0.1% TritonX-100-PBS and
699 finally permeabilized in 0.5% TritonX 100-PBS for 30 min. Following the blocking with
700 10% BSA in 0.1% Tween 20-PBS for 1h at room temperature, primary antibody
701 incubation in 10% BSA in 0.1% Tween 20-PBS was performed for overnight at 4°C. 3X
702 5 min 0.1% Tween 20-PBS washed intestines then were incubated in secondary

703 antibodies for 1h at room temperature. Specimens were finally mounted in Fluoromount-
704 G (Southern Biotech) and analyzed with confocal imaging. Primary antibodies: mouse
705 anti-Arm (Wang et al., 2016; N2 7A1, DSHB, 1:50), mouse anti-Prospero (Wang et al.,
706 2016; MR1A, DSHB, 1/50), mouse anti-GFP (GFP-12A6, DSHB, 1/100), mouse anti-β-
707 galactosidase (Tian et al., 2016); 401A, DSHB, 1/100), mouse anti-Delta (Wang et al.,
708 2016; C594.9B, DSHB, 1/100), rabbit anti-phosho-S10-Histone3 (Wang et al., 2016; 06-
709 570, Millipore, 1/1000). The secondary antibodies were Alexa fluorophores (Thermo
710 Fisher Scientific) and diluted as 1/1000.

711 **Quantification of Stat-GFP immunostaining intensity:** Images from R5 region were
712 taken with a 63x objective. Each STAT-GFP$^+$ stem cell was identified using Imaris
713 software (Bitplane). The main intensity in those cells within a field (40 μm x 40 μm)
714 surrounding an *Iduna* mutant clone or an equal field at least 50 μm away from the
715 mutant clone was measured. The relative intensity was calculated and shown in the
716 figure (Wang et al., 2016). Statistical analysis was performed with Prism software
717 (GraphPad).

718 **Immunoprecipitation:** S2R+ cells were seeded at 5x10^6 cells/10 cm^2 culture plates
719 and incubated overnight at 25^{0}C. Cells were then co-transfected with 5μg of each
720 plasmid by using Mirus-insect transfection reagent. Negative control was transfected
721 with empty plasmids. 48 hours later, transfected cells were harvested. The cell pellets
722 were washed within cold 1X PBS. This step was repeated 3 times. Pellets were re-
723 suspended in 600μl 1% Triton X-100 lysing buffer. Re-suspended pellets were
724 incubated on ice for 15 min and mixed gently and periodically. Total lysates were
725 centrifuged at 13,000 rpm at 4^{0}C for 30 minutes. The supernatant was removed and

726 100µl was stored as total lysate. 25µl Protein A/G (Thermo Scientific) beats were
727 washed with lysing buffer for 3 times. 200µl supernatant was incubated with the mixture
728 of washed protein A-G beads on a rotator at cold room for 30 minutes. In a parallel way,
729 25µl Protein A/G was washed with lysing buffer for 3 times. At the end of incubation
730 period, beads-supernatant mixture was centrifuged at 2,000 rpm at 4^0C for 1 minute.
731 Pre-cleaned supernatant was collected and added to beads. Antibody was added to
732 supernatant-beads and incubated at cold room on a rotator for 4 h. Beads-supernatant-
733 antibody mixture was centrifuged at 2,000 rpm at 4^0C for 1 minute and beads were
734 washed with lysing buffer for 3 times. In the final step, beads were re-suspended in 50µl
735 of 3X sample buffer to perform immunoblotting.

736 **Recombinant protein purification from S2R+ cells:** S2R+ cells were seeded at $5x10^6$
737 cells/10 cm^2 culture plates and incubated overnight at 25^0C. Then, flag or myc-tagged
738 gene of interests were transfected and based on the small tag, a recombinant protein
739 was immunoprecipitated with flag or myc agarose beads as described above. Finally, by
740 using flag or myc peptides, tagged proteins were eluted and quantified by BCA (Pierce,
741 ThermoFisher Scientific).

742 **Quantification and statistics:** ISC quantification, dissected midguts were stained with
743 Armadillo and Prospero. Images of the R5 region (Buchon et al., 2013) were obtained
744 with a 63X objective and total number of $Arm^+/Pros^-$ cells in a field were counted.
745 Quantifications of immunoblot were done with Image J. Student *t-test* and ANOVA were
746 used as statistical analysis and those were done with Prism (GraphPad) software.

747 **Author Contributions:** HS and YG designed the concept of the study. YG performed
748 all experiments. YG and HS jointly wrote the manuscript.

749 **Acknowledgments:** We would like to thank all previous and current members of the
750 Steller Lab for their helpful suggestions and discussions, especially Adi Minis and Junko
751 Shimazu for critical reading of the ms. We also thank Drs. Norbert Perrimon, Jean-Paul
752 Vincent, Wei Du, Jessica Treisman, and Steven X. Hou for sharing their published
753 *Drosophila* lines, the Bloomington Stock Center and the Vienna *Drosophila* Research
754 Center for the fly stocks, and the *Drosophila* Genomics Resource Center and
755 Developmental Studies Hybridoma Bank (DSHB) for reagents. This work was
756 supported by NIH grant RO1GM60124 to H.S.
757 The authors declare no competing interests.

758 **References**

759 Andreu P., Colnot, S., Godard, C., Gad, S., Chafey, P., Niwa-Kawakita, M., Laurent-
760 Puig, P., Kahn, A., Robine, S., Perret, C., Romagnolo, B. (2005). Crypt-restricted
761 proliferation and commitment to the Paneth cell lineage following Apc loss in the mouse
762 intestine. Development. 132(6):1443-51.
763
764 Bach, E.A., Ekas, L.A., Ayala-Camargo, A., Flaherty, M.S., Lee, H., Perrimon, N., and
765 Baeg, G.H. (2007). GFP reporters detect the activation of the *Drosophila* JAK/STAT
766 pathway in vivo. Gene Expr. Patterns *7*, 323–331.
767
768 Bai P. (2012). Biology of Poly(ADP-Ribose) Polymerases: The Factotums of Cell
769 Maintenance. Molecular Cell. 58-6; 947–958, 1.
770
771 Buchon, N., Osman, D., David, F.P.A., Yu Fang, H., Boquete, J.P., Deplancke, B., and
772 Lemaitre, B. (2013). Morphological and Molecular Characterization of Adult Midgut
773 Compartmentalization in *Drosophila*. Cell Rep. *3*, 1725–1738.
774
775 Callow, M.G., Tran, H., Phu, L., Lau, T., Lee, J., Sandoval, W.N., Liu, P.S., Bheddah,
776 S., Tao, J., Lill, J.R., et al. (2011). Ubiquitin ligase RNF146 regulates Tankyrase and
777 Axin to promote Wnt signaling. PLoS One 6(7): e22595
778
779 Chiang, Y.J., Hsiao, S.J., Yver, D., Cushman, S.W., Tessarollo, L., Smith, S., and
780 Hodes, R.J. (2008). Tankyrase 1 and Tankyrase 2 are essential but redundant for
781 mouse embryonic development. PLoS One *3*, e2639.
782
783 Cho-Park, P.F., and Steller, H. (2013). Proteasome regulation by ADP-ribosylation. Cell
784 *153*, 614–627.
785
786 Clevers, H., and Nusse, R. (2012). Wnt/β-catenin signaling and disease. Cell *149*,
787 1192–1205.
788
789 Collins, R.T., and Treisman, J.E. (2000). Osa-containing Brahma chromatin remodeling
790 complexes are required for the repression of Wingless target genes. Genes Dev. *14*,
791 3140–3152.
792
793 Cordero, J.B., Stefanatos, R.K., Scopelliti, A., Vidal, M., and Sansom, O.J. (2012).
794 Inducible progenitor-derived Wingless regulates adult midgut regeneration in
795 *Drosophila*. EMBO J. *31*, 3901–3917.
796
797 Croy, H.E., Fuller, C.N., Giannotti, J., Robinson, P., Foley, A.V.A., Yamulla, R.J.,
798 Cosgriff, S., Greaves, B.D., Von Kleeck, R.A., An, H.H., et al. (2016). The poly(ADP-
799 ribose) polymerase enzyme Tankyrase antagonizes activity of the β-catenin destruction
800 complex through ADP-ribosylation of Axin and APC2. J. Biol. Chem. *291*, 12747–12760.
801

802 DaRosa, P.A., Wang, Z., Jiang, X., Pruneda, J.N., Cong, F., Klevit, R.E., and Xu, W.
803 (2014). Allosteric activation of the RNF146 ubiquitin ligase by a polyADP-ribosylation
804 signal. Nature. *8*; 517(7533): 223.
805
806 Feng, Y., Li, X., Ray, L., Song, H., Qu, J., Lin, S., and Lin, X. (2014). The *Drosophila*
807 Tankyrase regulates Wg signaling depending on the concentration of dAxin. Cell.
808 Signal. *26*, 1717–1724.
809
810 Feng, Y., Li, Z., Lv, L., Du, A., Lin, Z., Ye, X., Lin, Y., Lin, X. (2018) Tankyrase regulates
811 apoptosis by activating JNK signaling in Drosophila. Biochem Biophys Res Commun.
812 Sep 18;503(4):2234-2239. doi: 10.1016/j.bbrc.2018.06.143. Epub 2018 Jul 9.
813
814 Fevr, T., Robine, S., Louvard, D., and Huelsken, J. (2007). Wnt/ β-catenin is essential
815 for intestinal homeostasis and maintenance of intestinal stem cells. Mol. Cell. Biol. *27*,
816 7551–7559.
817
818 Gerlach, J.P., Emmink, B.L., Nojima, H., Kranenburg, O., and Maurice, M.M. (2014).
819 Wnt signaling induces accumulation of phosphorylated β-catenin in two distinct cytosolic
820 complexes. Open Biol. *4*, 140120–140120.
821
822 Gibson, A.B., and Kraus, W.L. (2012). New insights into the molecular and cellular
823 functions of poly-(ADP-ribose) and PARPs Nature Reviews Molecular Cell Biology 13;
824 411–424.
825
826 Ghiglione, C., Devergne, O., Georgenthum, E., Carballès, F., Médioni, C., Cerezo, D.,
827 Noselli, S. (2002). The *Drosophila* cytokine receptor Domeless controls border cell
828 migration and epithelial polarization during oogenesis. Development *129*, 5437–5447.
829
830 Gratz, S.J., Cummings, A.M., Nguyen, J.N., Hamm, D.C., Donohue, L.K., Harrison,
831 M.M., Wildonger, J., and O'connor-Giles, K.M. (2013). Genome engineering of
832 *Drosophila* with the CRISPR RNA-guided Cas9 nuclease. Genetics *194*, 1029–1035.
833
834 Gratz, S.J., Ukken, F.P., Rubinstein, C.D., Thiede, G., Donohue, L.K., Cummings, A.M.,
835 and Oconnor-Giles, K.M. (2014). Highly specific and efficient CRISPR/Cas9-catalyzed
836 homology-directed repair in *Drosophila*. Genetics *196*, 961–971.
837
838 Hamada, F., Tomoyasu, Y., Takatsu, Y., Nakamura, M., Nagai, S.I., Suzuki, A., Fujita,
839 F., Shibuya, H., Toyoshima, K., Ueno, N., et al. (1999). Negative regulation of Wingless
840 signaling by D-Axin, a Drosophila homolog of Axin. Science. *283*, 1739–1742.
841
842 Herr, P., Hausmann, G., Basler, K. (2012). WNT secretion and signaling in human
843 disease. Trends Mol Med. (8):483-93.
844
845 Hsiao, S.J., Poitras, M.F., Cook, B.D., Liu, Y., and Smith, S. (2006). Tankyrase 2 poly-
846 (ADP-Ribose) polymerase domain-deleted mice exhibit growth defects but have normal
847 telomere length and capping. Mol. Cell. Biol. *26*, 2044–2054.

848
849 Huang, S.M.A., Mishina, Y.M., Liu, S., Cheung, A., Stegmeier, F., Michaud, G.A.,
850 Charlat, O., Wiellette, E., Zhang, Y., Wiessner, S., et al. (2009). Tankyrase inhibition
851 stabilizes Axin and antagonizes Wnt signaling. Nature *461*, 614–620.
852
853 Jiang, H., Patel P.H., Kohlmaier, A., Grenley, M.O., McEwen, D.G., Edgar, B.A. (2009).
854 Cytokine/Jak/Stat signaling mediates regeneration and homeostasis in the Drosophila
855 midgut. Cell. Jun 26;137(7):1343-55. doi: 10.1016/j.cell.2009.05.014.
856
857 Kinzler, K., Nilbert, M., Su, L., Vogelstein, B., Bryan, T., Levy, D., Smith, K., Preisinger,
858 A., Hedge, P., McKechnie, D., et al. (1991). Identification of FAP locus genes from
859 chromosome 5q21. Science. *253*, 661–665.
860
861 Korinek, V., Barker, N., Morin, P.J., van Wichen, D., de Weger, R., Kinzler, K.W.,
862 Vogelstein, B., and Clevers, H. (1997). Constitutive transcriptional activation by a beta-
863 catenin-Tcf complex in $APC^{-/-}$ colon carcinoma. Science *275*, 1784–1787.
864
865 Korinek, V., Barker, N., Moerer, P., Van Donselaar, E., Huls, G., Peters, P.J., and
866 Clevers, H. (1998). Depletion of epithelial stem-cell compartments in the small intestine
867 of mice lacking Tcf-4. Nat. Genet. *19*, 379–383.
868
869 Kramps, T., Peter, O., Brunner, E., Nellen, D., Froesch, B., Chatterjee, S., Murone, M.,
870 Züllig, S., and Basler, K. (2002). Wnt/Wingless signaling requires BCL9/legless-
871 mediated recruitment of pygopus to the nuclear β-catenin-TCF complex. Cell *109*, 47–
872 60.
873
874 Lee, E., Salic, A., Krüger, R., Heinrich, R., and Kirschner, M.W. (2003). The roles of
875 APC and Axin derived from experimental and theoretical analysis of the Wnt pathway.
876 PLoS Biol. *1*.
877
878 Li, V.S.W., Ng, S.S., Boersema, P.J., Low, T.Y., Karthaus, W.R., Gerlach, J.P.,
879 Mohammed, S., Heck, A.J.R., Maurice, M.M., Mahmoudi, T., et al. (2012). Wnt signaling
880 through inhibition of β-catenin degradation in an intact Axin1 Complex. Cell *149*, 1245–
881 1256.
882
883 Lin, G., Xu, N., and Xi, R. (2008). Paracrine Wingless signaling controls self-renewal of
884 *Drosophila* intestinal stem cells. Nature *455*, 1119–1123.
885
886 Lu, J., Ma, Z., Hsieh, J.C., Fan, C.W., Chen, B., Longgood, J.C., Williams, N.S.,
887 Amatruda, J.F., Lum, L., and Chen, C. (2009). Structure-activity relationship studies of
888 small-molecule inhibitors of Wnt response. Bioorganic Med. Chem. Lett. *19*, 3825–3827.
889
890 Markstein, M., Dettorre, S., Cho, J., Neumuller, R.A., Craig-Muller, S., and Perrimon, N.
891 (2014). Systematic screen of chemotherapeutics in *Drosophila* stem cell tumors. Proc.
892 Natl. Acad. Sci. *111*, 4530–4535.
893

894 Mattila, J., Kokki, K., Hietakangas, V., Boutros, M. (2018) Stem Cell Intrinsic
895 Hexosamine Metabolism Regulates Intestinal Adaptation to Nutrient Content. Dev
896 Cell. Sep 7. pii: S1534-5807(18)30681-6. doi: 10.1016/j.devcel.2018.08.011.
897
898 Matsumoto, Y., La Rose, J., Lim, M., Adissu, H.A., Law, N., Mao, X., Cong, F., Mera, P.,
899 Karsenty, G., Goltzman, D., et al. (2017). Ubiquitin ligase RNF146 coordinates bone
900 dynamics and energy metabolism. J. Clin. Invest. *127*, 2612–2625.
901
902 Matsumoto, Y., Larose, J., Kent, O.A., Lim, M., Changoor, A., Zhang, L., Storozhuk, Y.,
903 Mao, X., Grynpas, M.D., Cong, F., et al. (2017). RANKL coordinates multiple
904 osteoclastogenic pathways by regulating expression of ubiquitin ligase RNF146. J. Clin.
905 Invest. *127*, 1303–1315.
906
907 Micchelli, C.A., and Perrimon, N. (2006). Evidence that stem cells reside in the adult
908 *Drosophila* midgut epithelium. Nature *439*, 475–479.
909
910 Morin, P.J., Sparks, a B., Korinek, V., Barker, N., Clevers, H., Vogelstein, B., and
911 Kinzler, K.W. (1997). Activation of beta-catenin-Tcf signaling in colon cancer by
912 mutations in beta-catenin or APC. Science *275*, 1787–1790.
913
914 Nishisho, I., Nakamura, Y., Miyoshi, Y., Miki, Y., Ando, H., Horii, A., Koyama, K.,
915 Utsunomiya, J., Baba, S., and Hedge, P. (1991). Mutations of chromosome 5q21 genes
916 in FAP and colorectal cancer patients. Science. *253*, 665–669.
917
918 Nusse, R., and Clevers, H. (2017). Wnt/β-catenin signaling, disease, and emerging
919 therapeutic modalities. Cell *169*, 985–999.
920
921 Ohlstein, B., and Spradling, A. (2006). The adult *Drosophila* posterior midgut is
922 maintained by pluripotent stem cells. Nature *439*, 470–474.
923
924 Port, F., Chen, H.-M., Lee, T., and Bullock, S.L. (2014). Optimized CRISPR/Cas tools
925 for efficient germline and somatic genome engineering in *Drosophila*. Proc. Natl. Acad.
926 Sci. *111*, E2967–E2976.
927
928 Riffell J.L., Lord C.J, and Ashworth A. (2012). Tankyrase-targeted therapeutics:
929 expanding opportunities in the PARP family. Nature Reviews Drug Discovery. 11; 923–
930 936.
931
932 Rubinfeld, B., Robbins, P., El-Gamil, M., Albert, I., Porfiri, E., and Polakis, P. (1997).
933 Stabilization of beta-catenin by genetic defects in melanoma cell lines. Science *275*,
934 1790–1792.
935
936 Saito-Diaz, K., Benchabane, H., Tiwari, A., Tian, A., Li, B., Thompson, J.J., Hyde, A.S.,
937 Sawyer, L.M., Jodoin, J.N., Santos, E., et al. (2018). APC inhibits ligand-independent
938 Wnt signaling by the clathrin endocytic pathway. Dev. Cell *44*, 566–581.e8.
939

940 Salic, A., Lee, E., Mayer, L., and Kirschner, M.W. (2000). Control of β-catenin stability:
941 Reconstitution of the cytoplasmic steps of the Wnt pathway in *Xenopus* egg extracts.
942 Mol. Cell *5*, 523–532.
943
944 Theodosiou, N.A., and Xu, T. (1998). Use of FLP/FRT system to study *Drosophila*
945 development. Methods A Companion to Methods Enzymol. *14*, 355–365.
946
947 Tian, A., Benchabane, H., Wang, Z., and Ahmed, Y. (2016). Regulation of stem cell
948 proliferation and cell fate specification by Wingless/Wnt signaling gradients enriched at
949 adult intestinal compartment boundaries. PLoS Genet. *12*.
950
951 Wang, Z., Tian, A., Benchabane, H., Tacchelly-Benites, O., Yang, E., Nojima, H., and
952 Ahmed, Y. (2016a). The ADP-ribose polymerase Tankyrase regulates adult intestinal
953 stem cell proliferation during homeostasis in *Drosophila*. Development *143*, 1710–1720.
954
955 Wang, Z., Tacchelly-Benites, O., Yang, E., Thorne, C.A., Nojima, H., Lee, E., and
956 Ahmed, Y. (2016b). Wnt/wingless pathway activation is promoted by a critical threshold
957 of Axin maintained by the tumor suppressor APC and the ADP-ribose polymerase
958 Tankyrase. Genetics *203*, 269–281.
959
960 Xu, N., Wang, S.Q., Tan, D., Gao, Y., Lin, G., and Xi, R. (2011). EGFR, Wingless and
961 JAK/STAT signaling cooperatively maintain *Drosophila* intestinal stem cells. Dev. Biol.
962 *354*, 31–43.
963
964 Yang, E., Tacchelly-Benites, O., Wang, Z., Randall, M.P., Tian, A., Benchabane, H.,
965 Freemantle, S., Pikielny, C., Tolwinski, N.S., Lee, E., et al. (2016). Wnt pathway
966 activation by ADP-ribosylation. Nat. Commun. *7*.
967
968 Zeidler, M.P., Bach, E.A., and Perrimon, N. (2000). The roles of the *Drosophila*
969 JAK/STAT pathway. Oncogene *19*, 2598–2606.
970
971 Zhang, Y., Liu, S., Mickanin, C., Feng, Y., Charlat, O., Michaud, G.A., Schirle, M., Shi,
972 X., Hild, M., Bauer, A., et al. (2011). RNF146 is a poly-(ADP-ribose)-directed E3 ligase
973 that regulates Axin degradation and Wnt signaling. Nat. Cell Biol. *13*, 623–629.
974
975 Zhou, F., Rasmussen, A., Lee, S., and Agaisse, H. (2013). The UPD3 cytokine couples
976 environmental challenge and intestinal stem cell division through modulation of
977 JAK/STAT signaling in the stem cell microenvironment. Dev. Biol. *373*, 383–393.
978
979 Zoranovic, T., Grmai, L., and Bach, E. (2013). Regulation of proliferation, cell
980 competition, and cellular growth by the *Drosophila* JAK-STAT pathway. Jak-Stat *2*,
981 e25408.
982
983
984

Figure 1

A

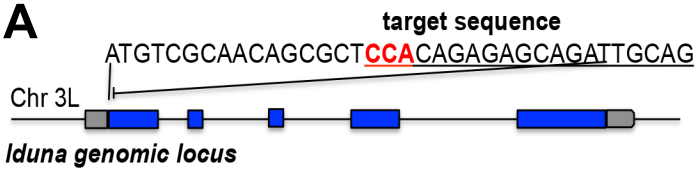

	Sequence	Deletion size(nt)
WT	ATGTCGCAACAGCGCT**CCA**CAGAGCAGATTGCAG	-
Mutant#17	ATGTCGCAACAGCGCTCCACAG---------GATTGCAG	(-4)
Mutant#78	ATGTCGCAACAGCGCTCCACAG-----CAGATTGCAG	(-2)

B

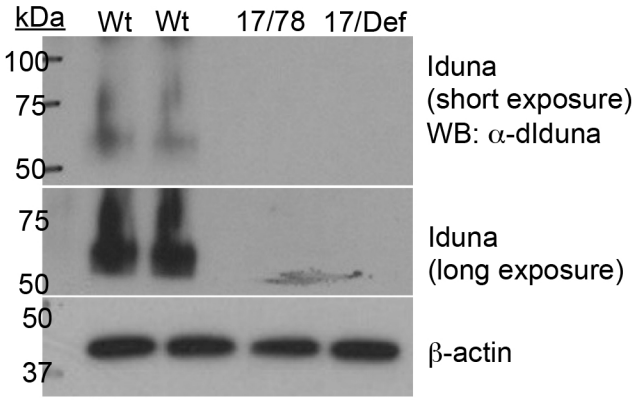

C

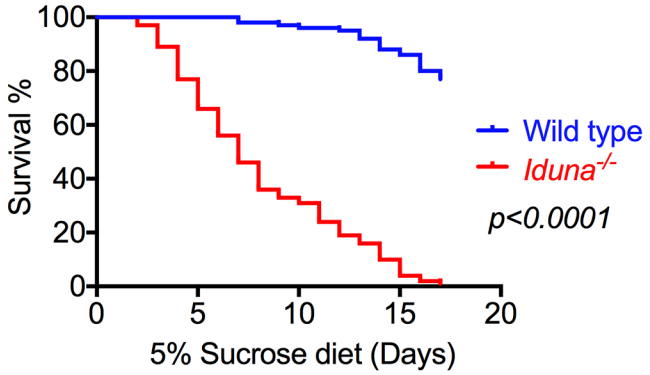

Figure 2

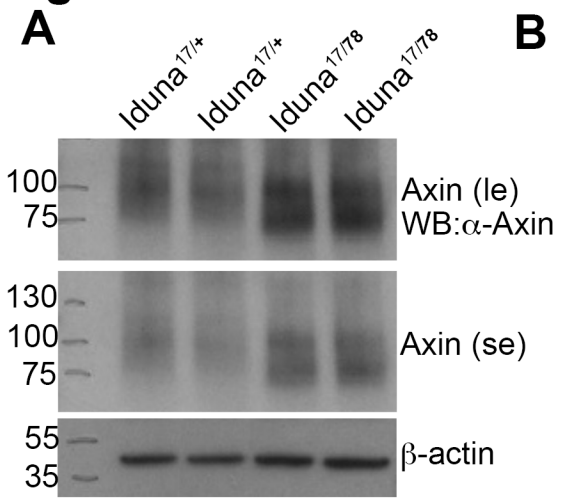
A
Iduna17/+
Iduna17/+
Iduna17/78
Iduna17/78
100
75
Axin (le)
WB:α-Axin
130
100
75
Axin (se)
55
35
β-actin

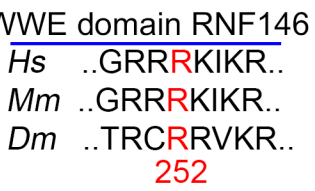
B
WWE domain RNF146
Hs ..GRRRKIKR..
Mm ..GRRRKIKR..
Dm ..TRCRRVKR..
252

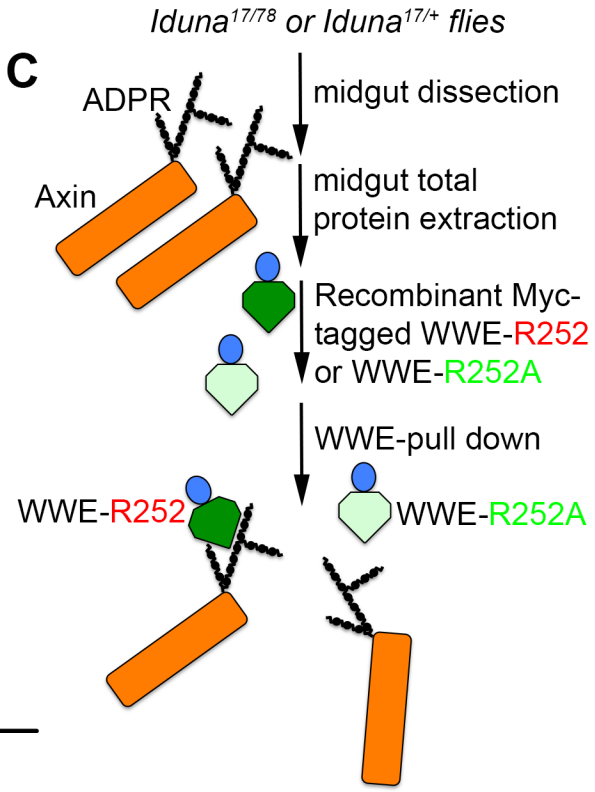
Iduna17/78 or Iduna17/+ flies
C
ADPR
Axin
midgut dissection
midgut total protein extraction
Recombinant Myc-tagged WWE-R252 or WWE-R252A
WWE-pull down
WWE-R252
WWE-R252A

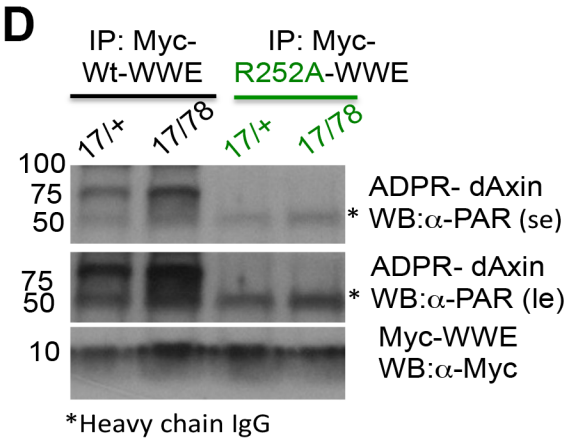
D
IP: Myc-Wt-WWE
IP: Myc-R252A-WWE
17/+
17/78
17/+
17/78
100
75
50
ADPR- dAxin
* WB:α-PAR (se)
75
50
ADPR- dAxin
* WB:α-PAR (le)
10
Myc-WWE
WB:α-Myc
*Heavy chain IgG

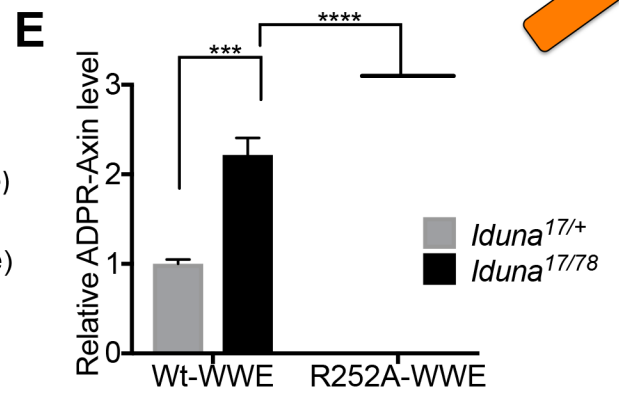
E
Relative ADPR-Axin level
0
1
2
3
***
****
Iduna17/+
Iduna17/78
Wt-WWE
R252A-WWE

Figure 3

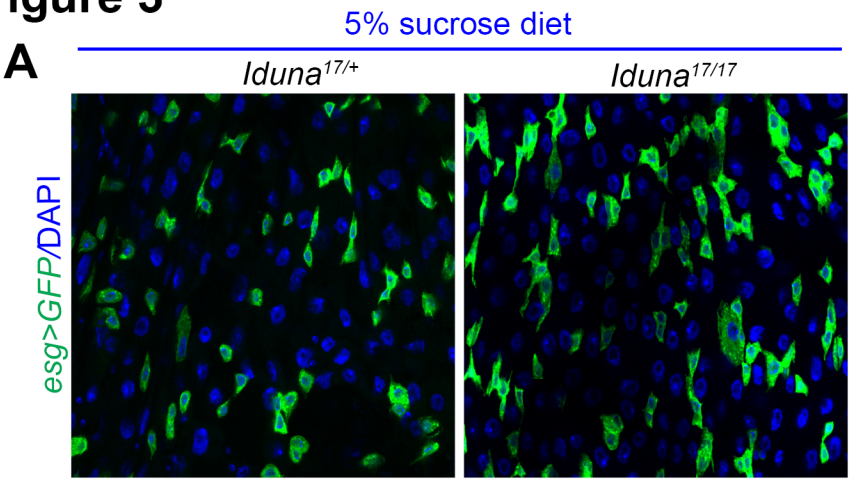
A
5% sucrose diet
Iduna17/+
Iduna17/17
esg>GFP/DAPI

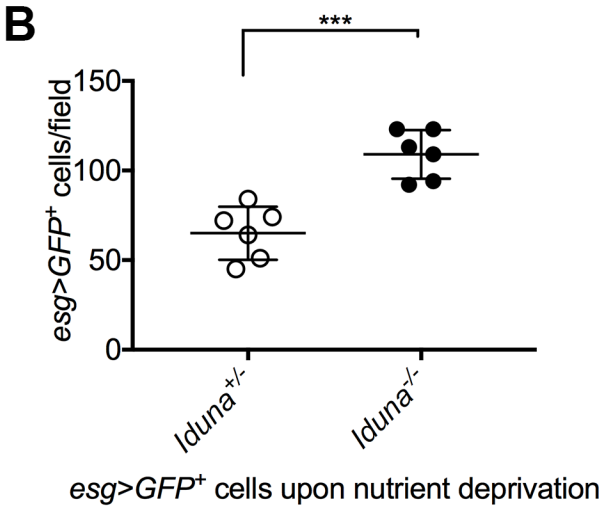
B
***
esg>GFP+ cells/field
150
100
50
0
Iduna+/-
Iduna-/-
esg>GFP+ cells upon nutrient deprivation

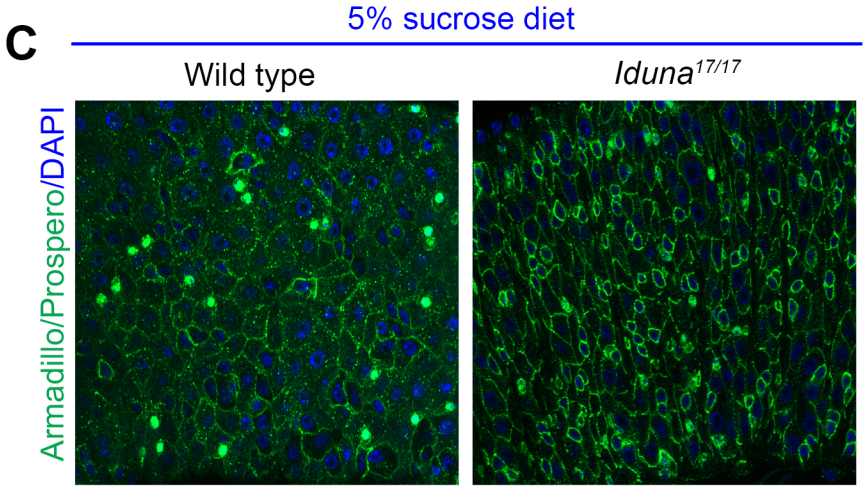
C
5% sucrose diet
Wild type
Iduna17/17
Armadillo/Prospero/DAPI

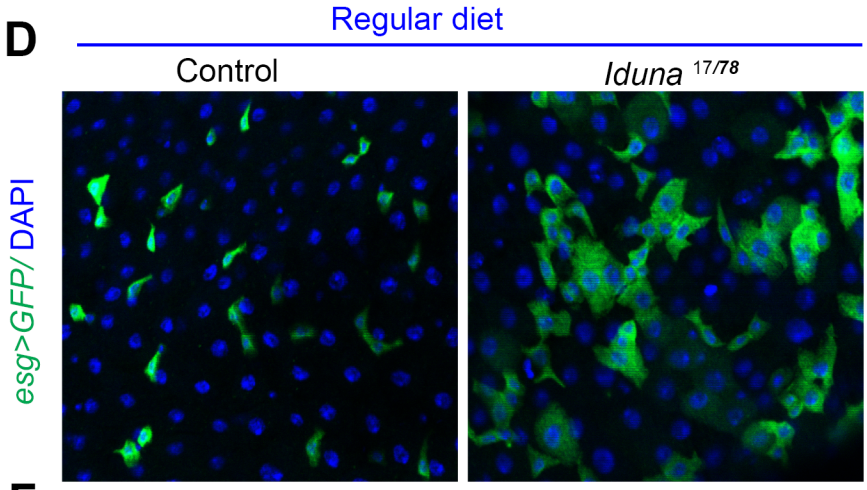
D
Regular diet
Control
Iduna 17/78
esg>GFP/ DAPI

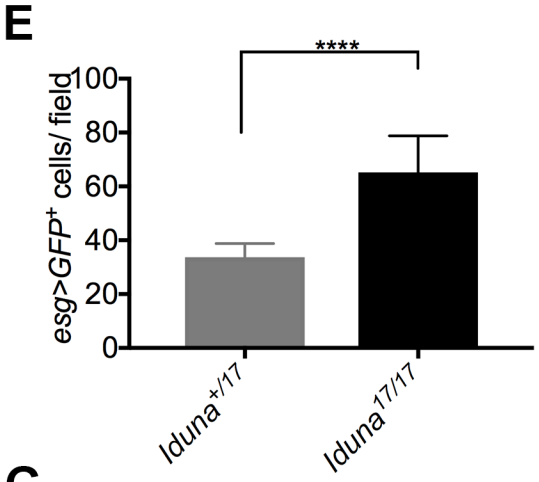
E
****
esg>GFP+ cells/ field
100
80
60
40
20
0
Iduna+/17
Iduna17/17

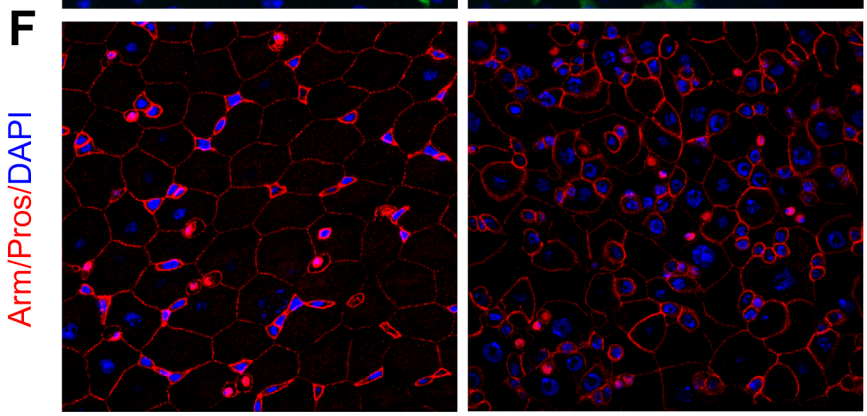
F
Arm/Pros/DAPI

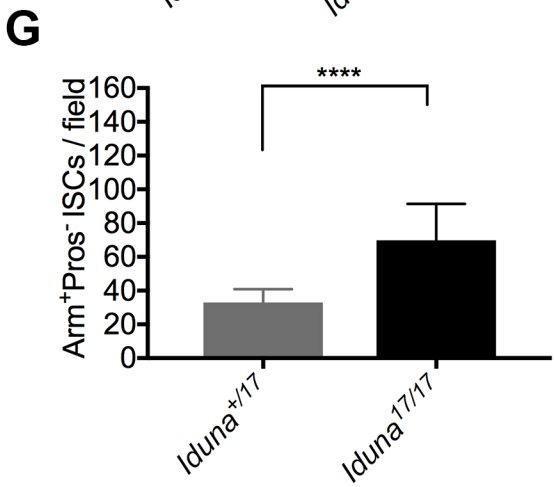
G
****
Arm+Pros- ISCs / field
160
140
120
100
80
60
40
20
0
Iduna+/17
Iduna17/17

Figure 4

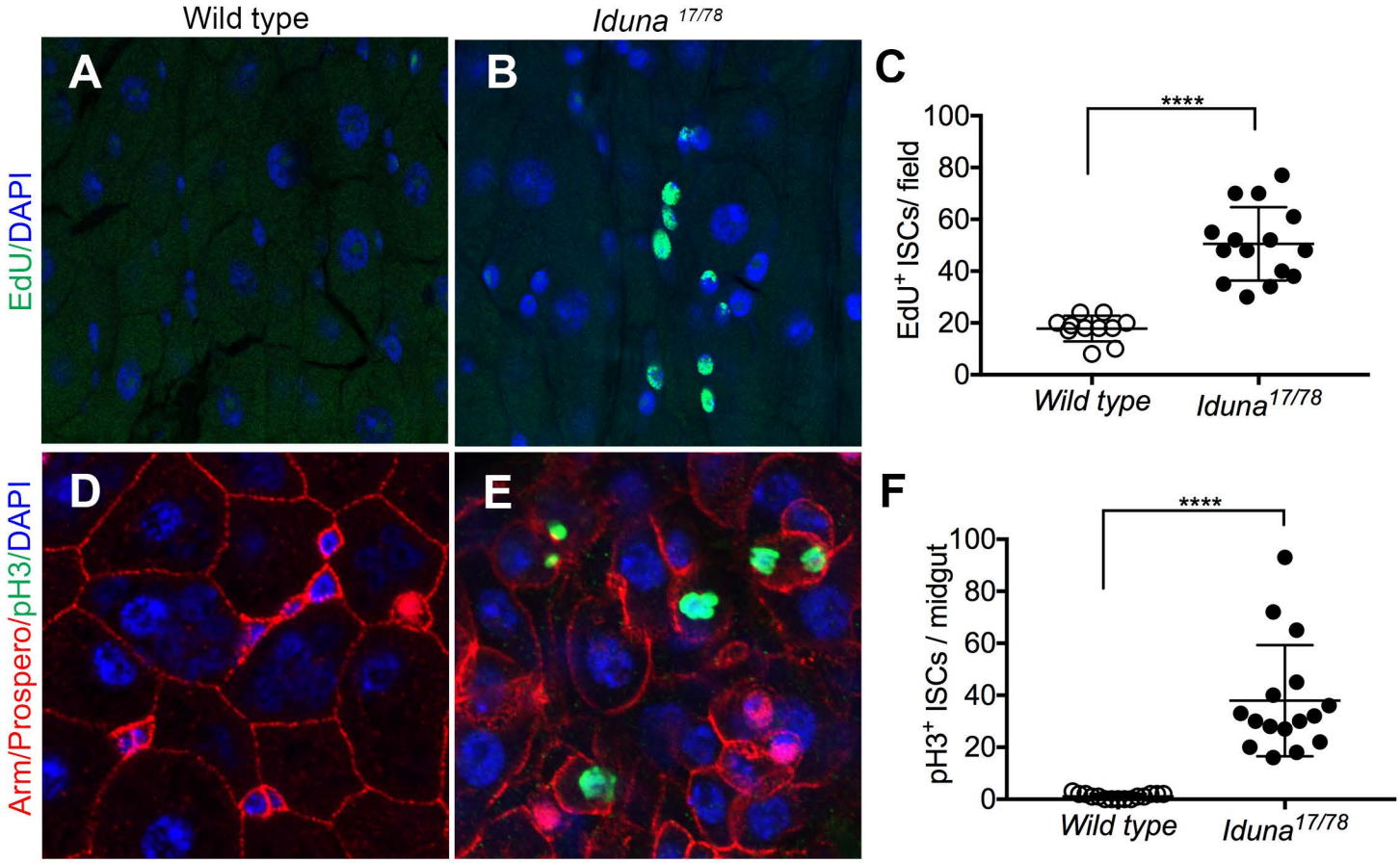
Wild type
Iduna 17/78
A
B
C
D
E
F
EdU/DAPI
Arm/Prospero/pH3/DAPI
EdU+ ISCs/ field
pH3+ ISCs / midgut
****
****
100
80
60
40
20
0
Wild type
Iduna17/78

Figure 5

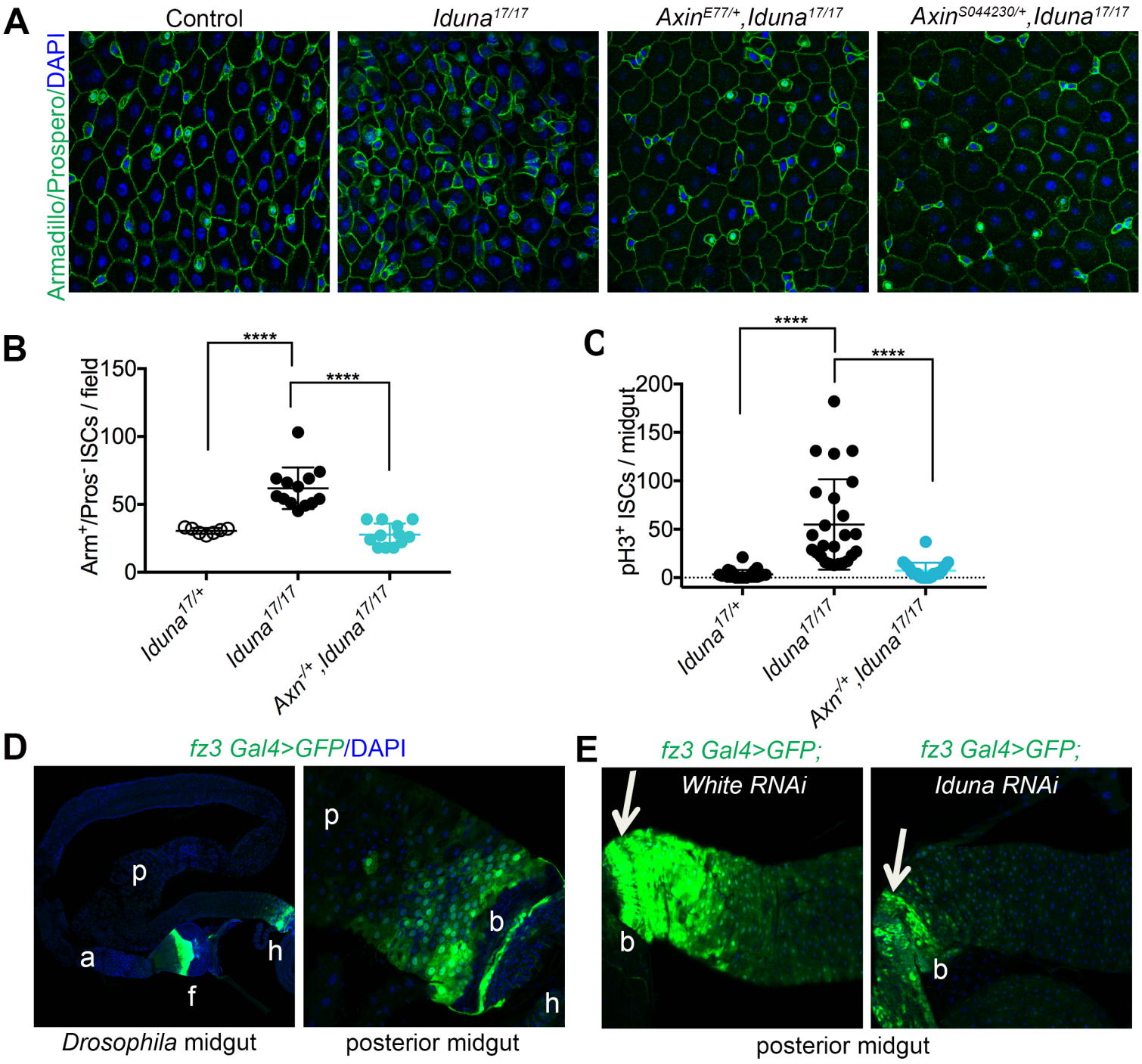
A
Control
Iduna17/17
AxinE77/+,Iduna17/17
AxinS044230/+,Iduna17/17
Armadillo/Prospero/DAPI
B
Arm+/Pros- ISCs / field
150
100
50
0
****
****
Iduna17/+
Iduna17/17
Axn-/+,Iduna17/17
C
pH3+ ISCs / midgut
200
150
100
50
0
****
****
Iduna17/+
Iduna17/17
Axn-/+,Iduna17/17
D
fz3 Gal4>GFP/DAPI
p
a
f
h
p
b
h
Drosophila midgut
posterior midgut
E
fz3 Gal4>GFP;
White RNAi
fz3 Gal4>GFP;
Iduna RNAi
b
b
posterior midgut

Figure 6

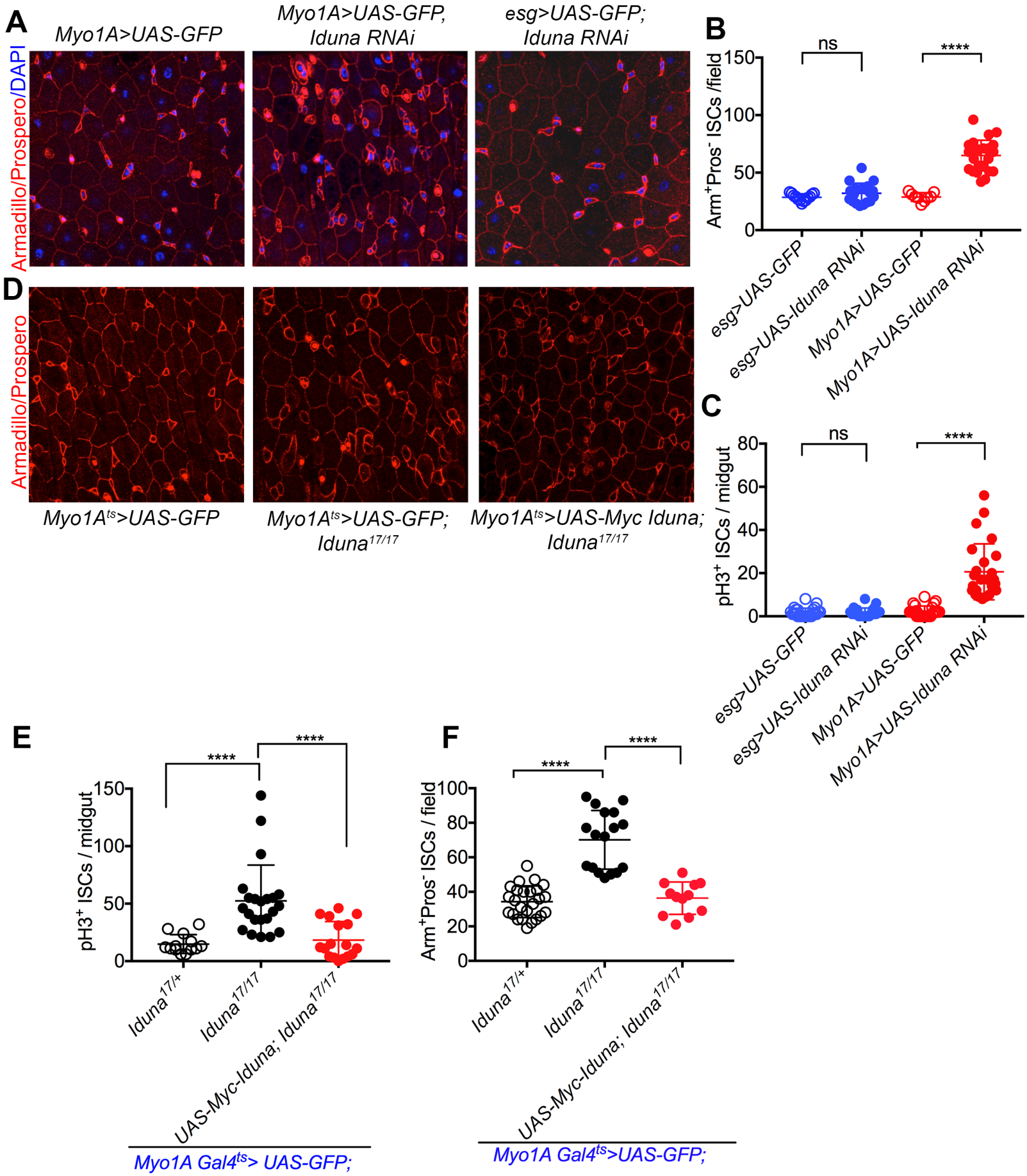
A
Myo1A>UAS-GFP
Myo1A>UAS-GFP, Iduna RNAi
esg>UAS-GFP; Iduna RNAi
Armadillo/Prospero/DAPI
B
ns
****
Arm+Pros- ISCs /field
150
100
50
0
esg>UAS-GFP
esg>UAS-Iduna RNAi
Myo1A>UAS-GFP
Myo1A>UAS-Iduna RNAi
D
Armadillo/Prospero
Myo1Ats>UAS-GFP
Myo1Ats>UAS-GFP; Iduna17/17
Myo1Ats>UAS-Myc Iduna; Iduna17/17
C
ns
****
pH3+ ISCs / midgut
80
60
40
20
0
esg>UAS-GFP
esg>UAS-Iduna RNAi
Myo1A>UAS-GFP
Myo1A>UAS-Iduna RNAi
E
****
****
pH3+ ISCs / midgut
150
100
50
0
Iduna17/+
Iduna17/17
UAS-Myc-Iduna; Iduna17/17
Myo1A Gal4ts> UAS-GFP;
F
****
****
Arm+Pros- ISCs / field
100
80
60
40
20
0
Iduna17/+
Iduna17/17
UAS-Myc-Iduna; Iduna17/17
Myo1A Gal4ts>UAS-GFP;

Figure 7

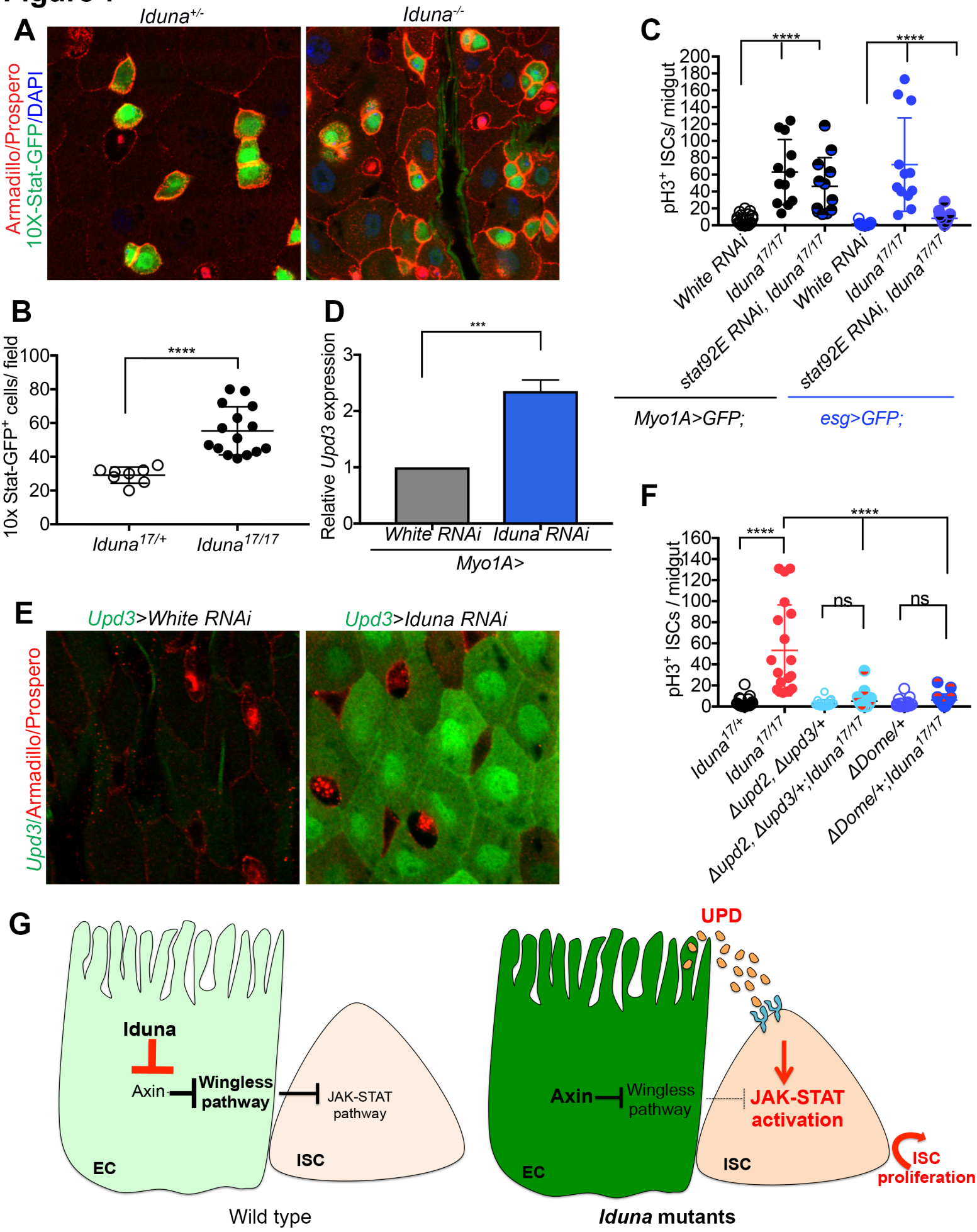
A
Iduna+/-
Iduna-/-
Armadillo/Prospero
10X-Stat-GFP/DAPI
B
10x Stat-GFP+ cells/ field
****
Iduna17/+
Iduna17/17
C
pH3+ ISCs/ midgut
****
****
White RNAi
Iduna17/17
Iduna17/17
stat92E RNAi, Iduna17/17
White RNAi
Iduna17/17
stat92E RNAi, Iduna17/17
Myo1A>GFP;
esg>GFP;
D
Relative Upd3 expression
***
White RNAi
Iduna RNAi
Myo1A>
E
Upd3>White RNAi
Upd3>Iduna RNAi
Upd3/Armadillo/Prospero
F
pH3+ ISCs / midgut
****
****
ns
ns
Iduna17/+
Iduna17/17
Δupd2, Δupd3/+
Δupd2, Δupd3/+;Iduna17/17
ΔDome/+
ΔDome/+;Iduna17/17
G
Iduna
Axin
Wingless pathway
JAK-STAT pathway
EC
ISC
Wild type
UPD
Axin
Wingless pathway
JAK-STAT activation
EC
ISC
ISC proliferation
Iduna mutants

Supplementary Figure Legends

Figure S1: *Iduna* inactivation does not cause developmental defects in *Drosophila.* A- Identification of *Iduna*^{17} and *Iduna*^{78} mutant alleles. *Iduna*^{17} had no detectable *Iduna* transcripts, and Iduna^{78} had severely reduced *Iduna* mRNA based on RT-PCR. 7 day-old adult females were analyzed for expressions of *Iduna*, *Ribosomal protein 49* (a house keeping gene) and *Ornitate aminotransferase.* **B-** *Iduna* mutants did not have defects in hatching their eggs. n>250 for each genotype. **C-** *Iduna* transheterozygous mutants did not have defects in hatching their eggs. n>100 for each genotype. **D-** *Iduna* mutants do not have nutrient uptake *Iduna* mutant larvae could be pupated and enclosed to adult *Drosophila.* n>100 for each genotype. **E-** There is no decrease in food intake in *Iduna* mutant when flies kept under the regular diet. Quantification of adult fly nutrient uptake by a calorimetric assay from regular dietary condition in *Iduna* mutants and Oregon R.

Figure S2: *Iduna* depletion leads to increased Axin and Tankyrase protein levels. A- Mis-expression of GFP-Axin in adult eyes did not result in obvious eye phenotype. Five day-old adult male eyes were imaged. **B-** Mis-expressed Tankyrase however led to rough eye. *Iduna* inactivation promotes the eye phenotype. Five day-old adult male eyes were imaged. **C-** *Iduna* inactivation leads to mis-expressed GFP-Axin elevation. A UAS-GFP-Axin reporter transgene was expressed under *GMR* driver in the *Iduna* mutants or wild type. **D-** *Iduna* mutants had 2.5-fold increased GFP-Axin protein. Quantification of mis-expressed GFP-Axin immunoblottings. Results are based on two repeats of

24 independent replicates and Axin protein levels were normalized to β-actin. **E-**
25 Flag- tagged mis-expressed TNKS protein accumulates in *Iduna* mutants. A
26 UAS-Flag-TNKS reporter transgene was expressed under the *GMR-Gal4* driver
27 in *Iduna* mutants or wild type. **F**- *Iduna* mutants had 3.5-fold increased levels of
28 flag-tagged TNKS. Quantification of Flag-TNKS immunoblottings. Five day-old
29 adult male heads were dissected and 20μg of total protein lysates were analyzed
30 by immunoblotting to assess the levels of GFP-Axin or Flag-tagged TNKS using
31 α-GFP or α-flag antibodies, respectively. Western blot quantification was
32 performed based on two independent experimental replicates, and protein levels
33 were normalized with β-actin. Oregon R flies were used as a wild type control.
34 Flies were fed with regular diet at 24-25°C.

35 **Figure S3: *Iduna* inactivation causes increased mis-expressed Axin protein**
36 **levels in the midgut.**

37 **A-** *Iduna* mutant midguts had elevated mis-expressed GFP-Axin protein. Midguts
38 of 7 day-old adult females, which were expressing GFP-Axin under the
39 temperature sensitive *Myo1A-Gal4* driver, were dissected, lysed and analyzed by
40 GFP immunoblotting. *Iduna* mutants had more Axin protein compared to the wild
41 type. 20μg total intestinal lysates were analyzed by GFP immunoblotting and α-
42 tubulin was used as a loading control. **B-** Loss-of-*Iduna* resulted in 2.2-fold GFP-
43 Axin accumulation in the midgut. Western blot quantification was performed
44 based on two independent experimental replicates, and protein levels were
45 normalized to α-tubulin. **C-** *Iduna* mutant clones have elevated mis-expressed
46 GFP-Axin compared to their WT neighbours. A UAS-GFP-Axin transgene was

47 expressed under the temperature sensitive *Myo1A-Gal4* driver in the FRT80B-
48 *Iduna*^{17} mutant. Midgut mutant clones were induced during larval development by
49 daily incubation at 37°C for 1h. Adult female FRT80B-Nls-Red/FRT80B-*Iduna*^{17}
50 flies were collected after eclosion, incubated at 29°C and analyzed on day 7.
51 Unlabeled cells represent *Iduna* mutant clones, whereas cells stained for nuclear
52 RFP are either wild type or *Iduna* heterozygous. *p<0.001* is indicated as *** and
53 *p<0.0001* was marked as ****.

54 **Figure S4: Iduna is not required for differentiation of ISC. A-** Intestinal stem
55 cells in the *Drosophila* midgut give rise to enterocytes and enteroendocrine cells.
56 ISCs give rise to two different types of daughter progenitors, undifferentiated
57 enteroblasts (EBs) and pre-enteroendocrine cells (Pre-EE). EBs and pre-EEs
58 differentiate into enterocytes (ECs) and enteroendocrine (EEs) cells,
59 respectively. **B-** ISCs and ECs can be distinguished by their cell sizes, high level
60 of membrane-associated Armadillo, and lack of nuclear Prospero. On the other
61 hand, differentiated EEs are small and can be identified by nuclear Prospero
62 staining. Finally, small-sized ISCs are stained with Armadillo but not with nuclear
63 Prospero. In the image, small ISCs were co-stained with escargot (green), and
64 Armadillo (red). On the other hand, small EEs were shown with the red arrow and
65 stained with Armadillo (red) and nuclear Prospero (red). Bigger cells are
66 enterocytes whose cell membrane is stained with Armadillo (red). DAPI staining
67 in blue marks the cell nucleus. Flies were fed with regular diet at 24-25°C.*Iduna*
68 mutants contain slightly more cells in their midgut. It appears that an increase in
69 ISC number is responsible for this effect. **C-E-** No differences in the numbers of

70 enterocytes and enteroendocrine cells were observed in *Iduna* mutants. **F-** Iduna
71 is not required for the differentiation of stem cells into enterocytes. Enterocytes
72 were marked with GFP expressed under the control of enterocyte specific driver,
73 *Myo1A-Gal4*. 7d- old mutant clones were analyzed. Control cells are shown with
74 nuclear RFP, and *Iduna* mutant clones are marked with a white line. **G-** Genetic
75 depletion of *Iduna* did not affect the differentiation of ISCs into enteroendocrine
76 cells. Mutant clones in 7d-old adult midguts were analyzed with Prospero
77 staining. Small nuclear Prospero-positive EE cells are labeled with yellow arrows
78 in *Iduna* mutant clones. Control cells are labeled with nuclear RFP, and mutant
79 clones are marked with a white line. Flies were fed with regular diet at 24-25°C.

80 **Figure S5: RNAi-mediated *Iduna* depletion in enterocytes does not cause**
81 **mortality upon nutrient deprivation. A-** Three different *Iduna* RNAi lines were
82 expressed under the *Myo1A* driver. *White* RNAi was used as a control. **B-** There
83 was no significant change on the mean lifespan between *white* and *Iduna* RNAi
84 expressing flies. n=60 for each genotype. **C-** *Iduna* inactivation in enteroblast
85 does not lead to increased lethality upon 5% sucrose diet at 28°C. n=70 for each
86 genotype. **D-** Ectopic expression of *Iduna* under Myo1A driver in enterocytes
87 does not rescue elevated mortality of *Iduna* mutants under reduced nutrient diet.
88 Two-day old mutant or wild type female flies were collected and kept on 5%
89 sucrose diet at 28°C for the experiment in A-D**. E-** Enterocyte specific ectopic
90 expression of I*duna* rescues the hyper-proliferation of midgut stem cells upon
91 nutrient deprivation. 2 day-old females were collected at 24-25°C and their

92 regular diet was replaced with 5% sucrose diet at 28°C. 9 day-old female flies
93 were examined with α-Armadillo and Prospero antibodies.

94 **Figure S6: Under regular physiological conditions, the Stat-GFP reporter is**
95 **mainly expressed in midgut stem cells and enteroblasts . A-** 10x Stat-GFP
96 reporter was mainly positive in small sized cell populations but Prospero stained
97 enteroendocrine cells were negative for Stat-GFP in the midguts. **B-** Delta-lacZ
98 positive but Prospero negative cells were mainly positive for Stat-GFP
99 expression**.** It was also indicated with the white arrows that a small population of
100 cells, which were small-sized and GFP positive but Delta-lacZ negative. Those
101 could be undifferentiated progenitors like enteroblast cells. **C-** Armadillo positive
102 Prospero negative small sized stem and progenitor cells have Stat-GFP reporter
103 activity. 5 day-old female flies were dissected and stained with α-Armadillo and
104 Prospero antibodies.

105 **Figure S7: *Iduna* mutants have increased numbers of Stat-GFP positive**
106 **cells.**
107 **A**- *Iduna* mutant clones had elevated Stat-GFP signaling in ISCs. *10X-Stat-GFP*
108 is a reporter for STAT signaling activity. *Iduna* mutant clones displayed strongly
109 increased staining of this reporter. 7 day-old females were dissected and the
110 posterior midguts were analyzed. **B**- Quantification of Stat-GFP reporter
111 expression in *Iduna* mutant clones. GFP intensity was measured with Image J
112 and normalized with control cells. *Iduna* mutant clones showed 4-5 fold higher
113 reporter expression. **C- E-** *Iduna* mutants have more Stat-GFP positive stem cells
114 and progenitors in the midguts. 7 day-old females were dissected and the

115 posterior midguts were analyzed by confocal microscopy. n>6 for each genotype.
116 *p<0.0001* is indicated as ****. **F-** Delta protein is elevated in the midguts of *Iduna*
117 mutants. 7 day-old females were dissected and the midguts were stained for
118 Delta. Flies were collected and kept on regular diet at 24-25°C.
119
120 **Figure S8: RNAi-mediated *Iduna* depletion increases *Upd3>GFP* reporter**
121 **activity. A-** Knock-down of *Iduna* results in upregulation of *Upd3*. *Iduna* was
122 down-regulated by two different UAS-RNAi lines (#36029 and #40882) under
123 *Upd3-Gal4 driver*. *Upd3>GFP* was used as a reporter for *Upd3* gene expression.
124 *White RNAi* served as control. **B-C-** *Upd3 was* upregulated in the enterocytes.
125 Dissected midguts were stained with α–Armadillo and Prospero antibodies. ECs
126 were *Upd3>GFP* expressing cells but EEs and ISCs not. 3 day-old female flies
127 were dissected and their posterior midguts were analyzed by confocal
128 microscopy.
129
130
131
132
133

Figure S1

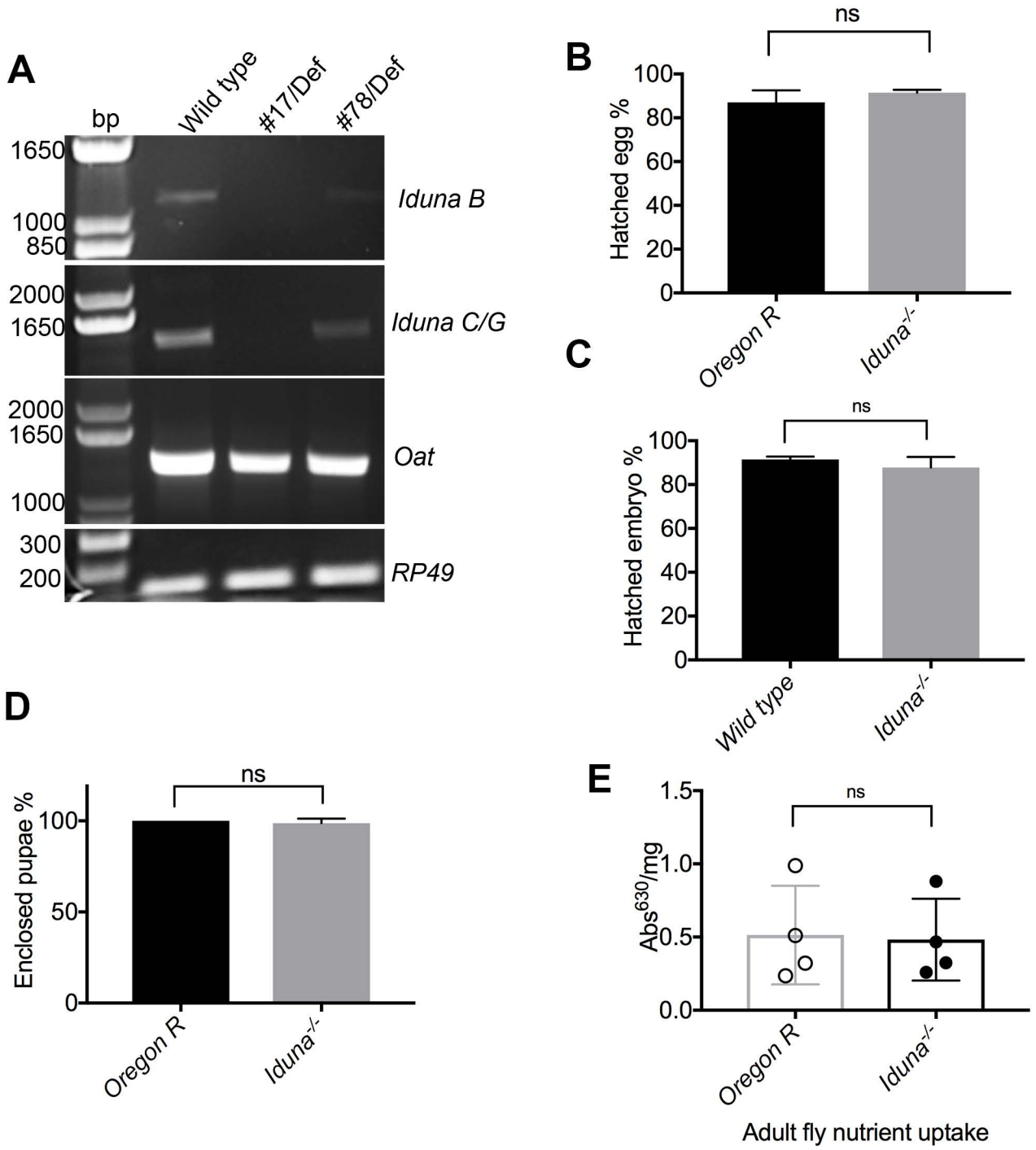
A
bp
Wild type
#17/Def
#78/Def
1650
1000
850
Iduna B
2000
1650
Iduna C/G
2000
1650
1000
Oat
300
200
RP49
B
ns
Hatched egg %
100
80
60
40
20
0
Oregon R
Iduna-/-
C
ns
Hatched embryo %
100
80
60
40
20
0
Wild type
Iduna-/-
D
ns
Enclosed pupae %
100
50
0
Oregon R
Iduna-/-
E
ns
Abs630/mg
1.5
1.0
0.5
0.0
Oregon R
Iduna-/-
Adult fly nutrient uptake

Figure S2

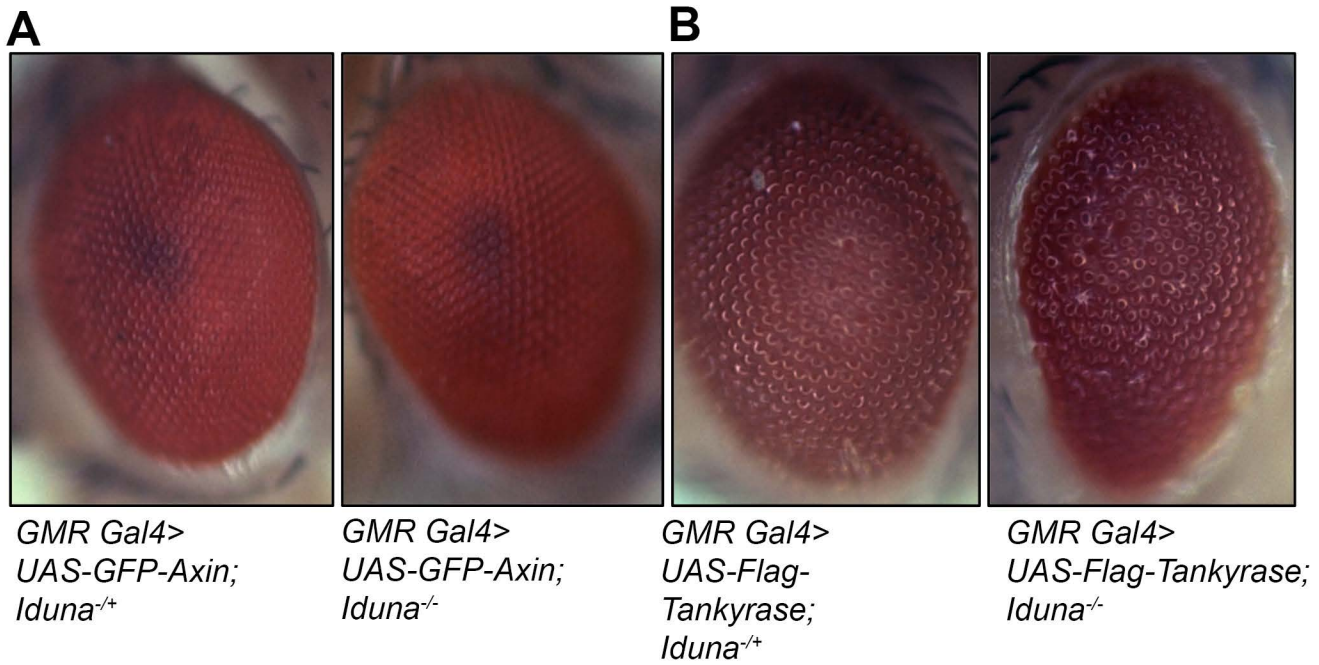
A
B
GMR Gal4> UAS-GFP-Axin; Iduna-/+
GMR Gal4> UAS-GFP-Axin; Iduna-/-
GMR Gal4> UAS-Flag-Tankyrase; Iduna-/+
GMR Gal4> UAS-Flag-Tankyrase; Iduna-/-

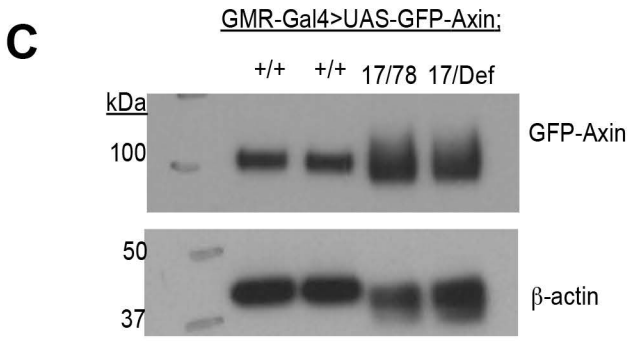
C
GMR-Gal4>UAS-GFP-Axin;
+/+
+/+
17/78
17/Def
kDa
100
50
37
GFP-Axin
β-actin

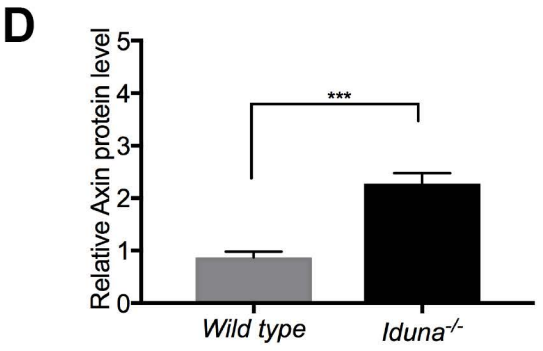
D
Relative Axin protein level
0
1
2
3
4
5
***
Wild type
Iduna-/-

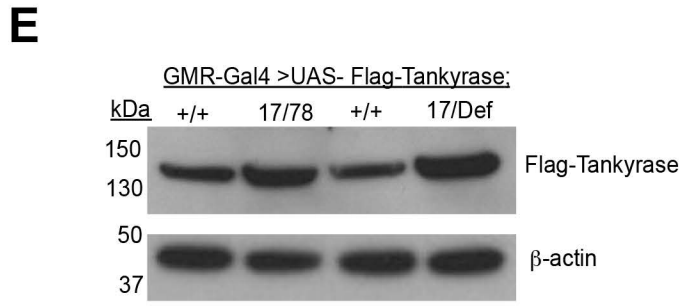
E
GMR-Gal4 >UAS- Flag-Tankyrase;
kDa
+/+
17/78
+/+
17/Def
150
130
50
37
Flag-Tankyrase
β-actin

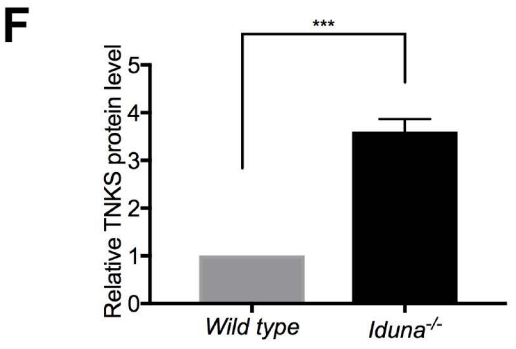
F
Relative TNKS protein level
0
1
2
3
4
5
***
Wild type
Iduna-/-

Figure S3

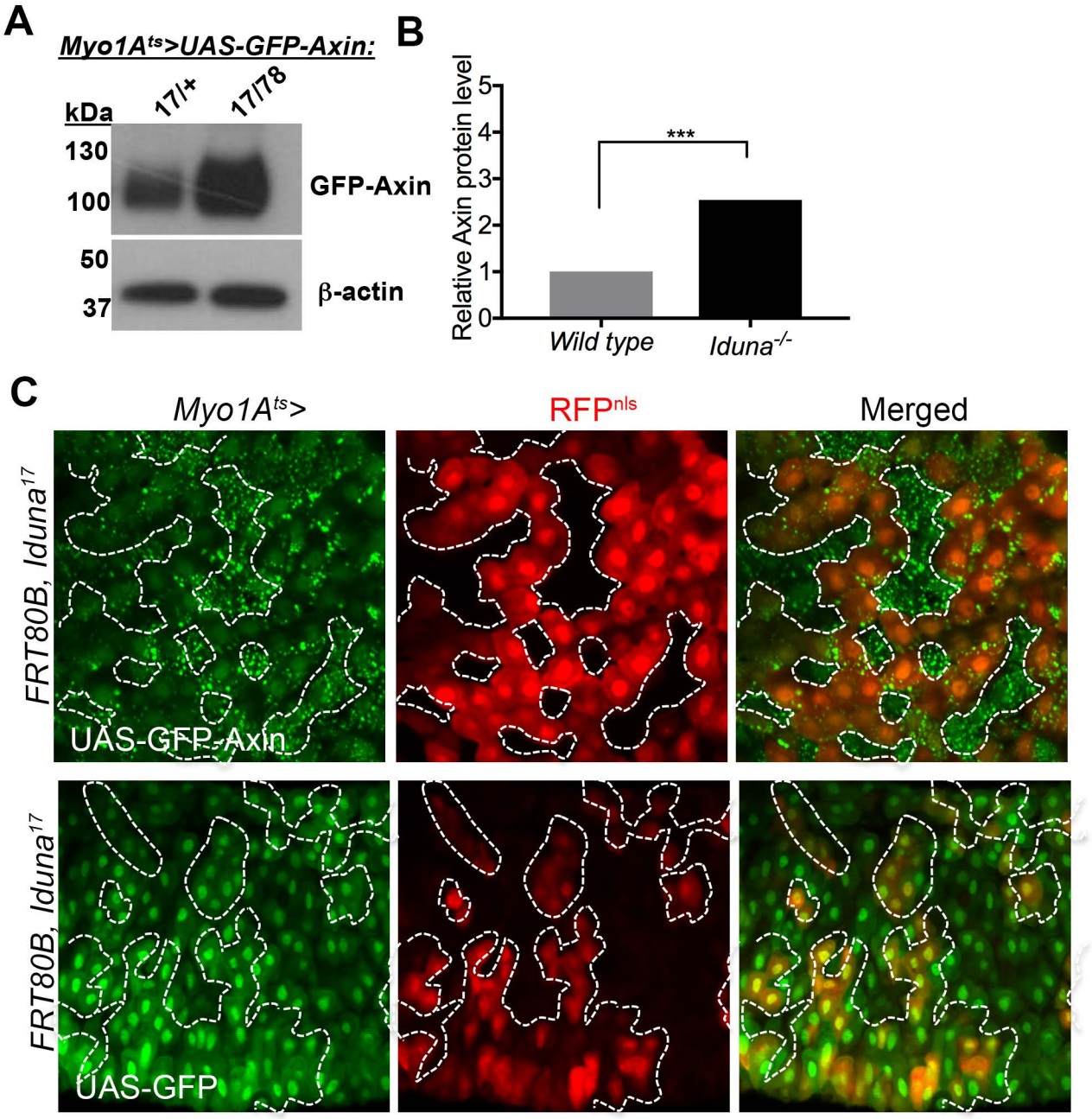
A
Myo1A^ts>UAS-GFP-Axin:
kDa
17/+
17/78
130
100
GFP-Axin
50
37
β-actin
B
Relative Axin protein level
5
4
3
2
1
0
***
Wild type
Iduna-/-
C
Myo1A^ts>
RFP^nls
Merged
FRT80B, Iduna17
UAS-GFP-Axin
FRT80B, Iduna17
UAS-GFP

Figure S4

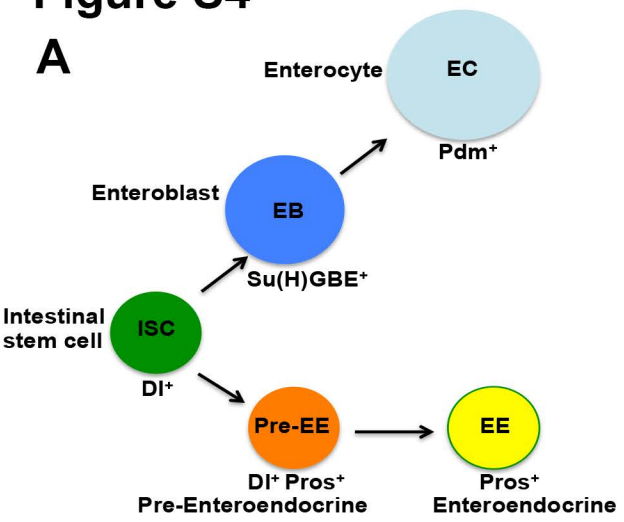
A
Enterocyte
EC
Pdm+
Enteroblast
EB
Su(H)GBE+
Intestinal stem cell
ISC
Dl+
Pre-EE
Dl+ Pros+
Pre-Enteroendocrine
EE
Pros+
Enteroendocrine

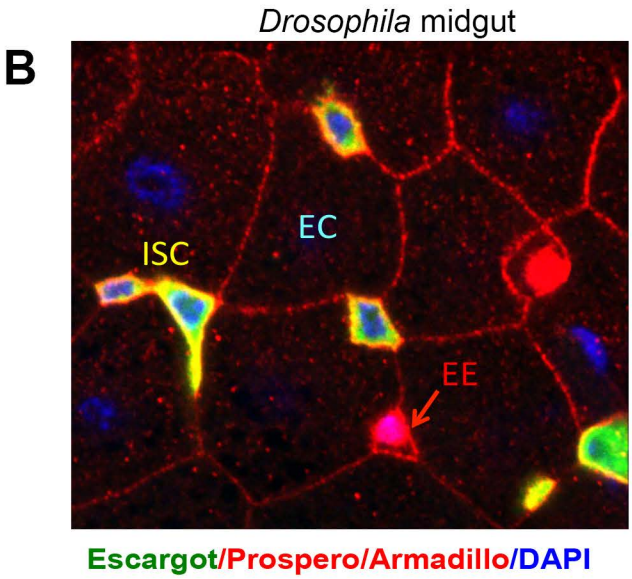
B
Drosophila midgut
ISC
EC
EE
Escargot/Prospero/Armadillo/DAPI

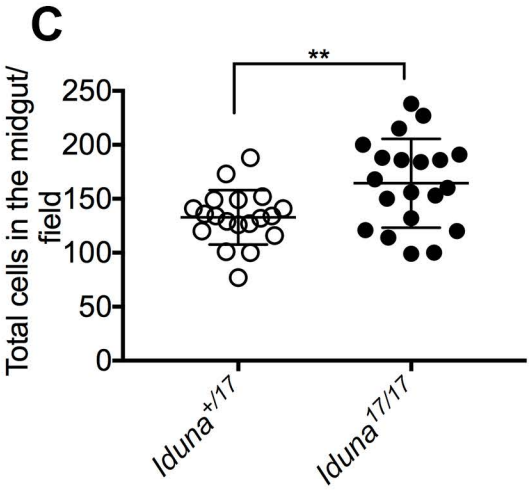
C
**
Total cells in the midgut/ field
250
200
150
100
50
0
Iduna+/17
Iduna17/17

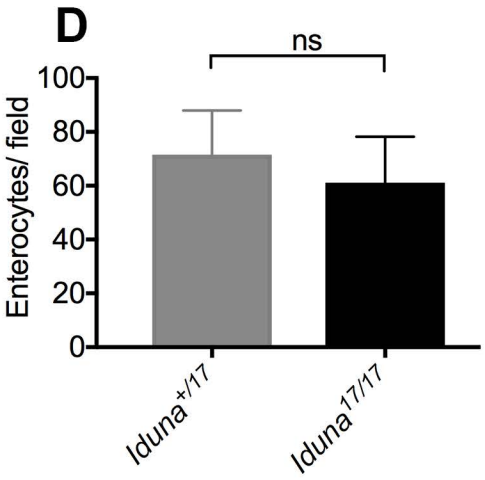
D
ns
Enterocytes/ field
100
80
60
40
20
0
Iduna+/17
Iduna17/17

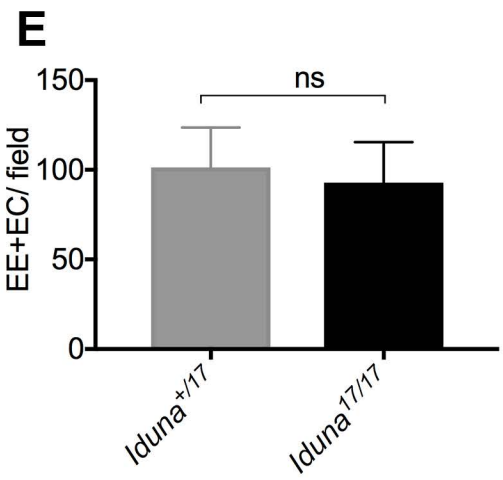
E
ns
EE+EC/ field
150
100
50
0
Iduna+/17
Iduna17/17

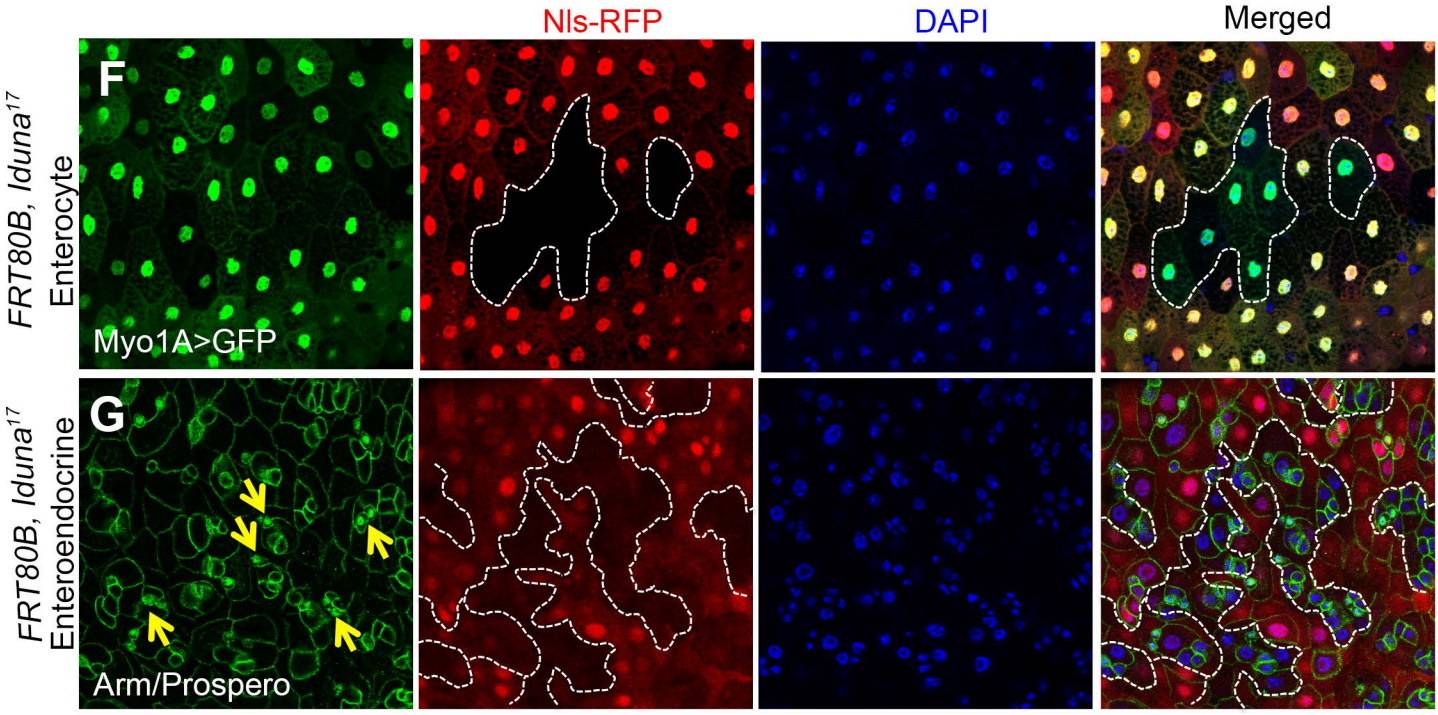
Nls-RFP
DAPI
Merged
F
FRT80B, Iduna17
Enterocyte
Myo1A>GFP
G
FRT80B, Iduna17
Enteroendocrine
Arm/Prospero

Figure S5

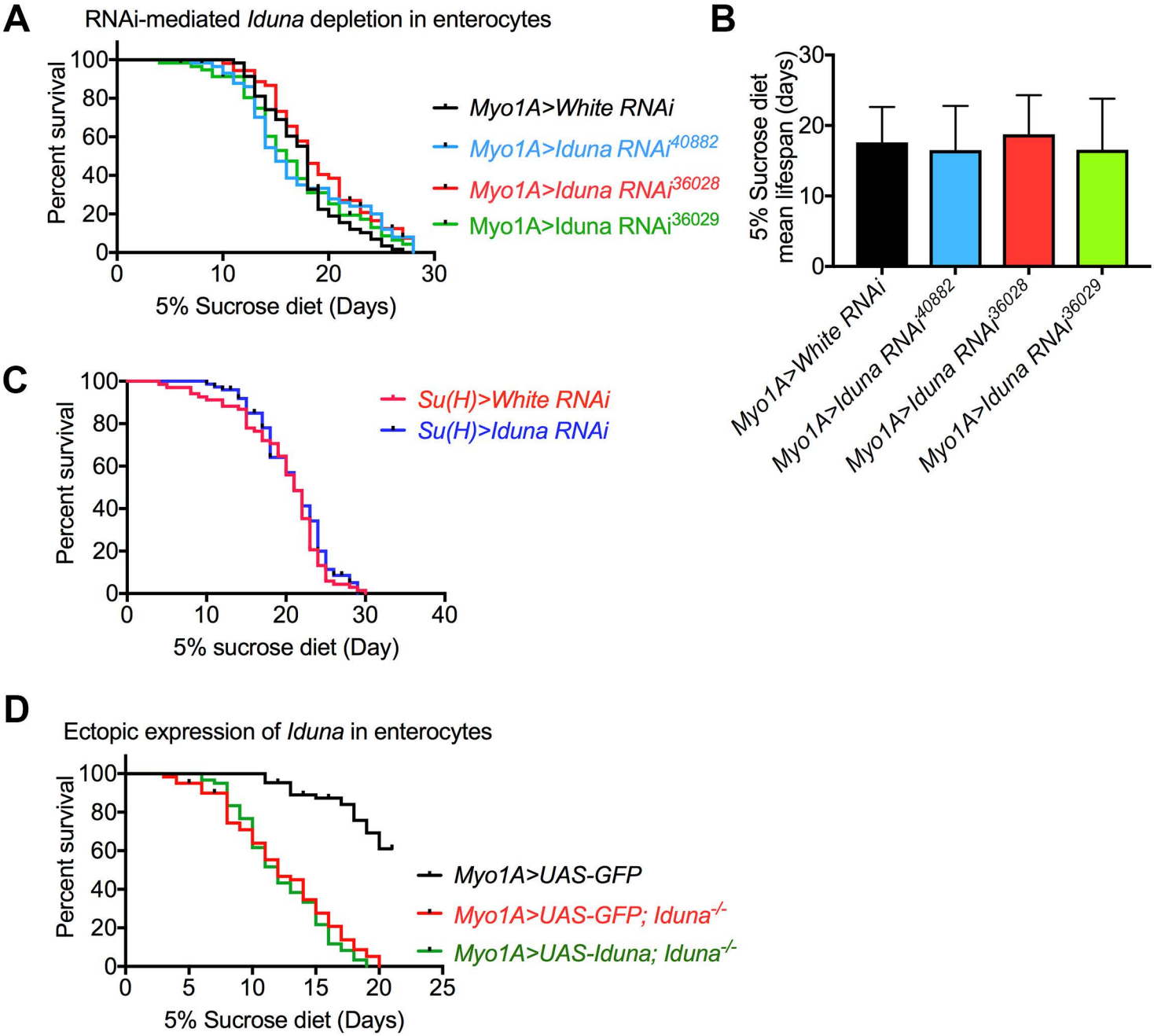
A
RNAi-mediated Iduna depletion in enterocytes
Percent survival
5% Sucrose diet (Days)
Myo1A>White RNAi
Myo1A>Iduna RNAi40882
Myo1A>Iduna RNAi36028
Myo1A>Iduna RNAi36029
B
5% Sucrose diet mean lifespan (days)
Myo1A>White RNAi
Myo1A>Iduna RNAi40882
Myo1A>Iduna RNAi36028
Myo1A>Iduna RNAi36029
C
Percent survival
5% sucrose diet (Day)
Su(H)>White RNAi
Su(H)>Iduna RNAi
D
Ectopic expression of Iduna in enterocytes
Percent survival
5% Sucrose diet (Days)
Myo1A>UAS-GFP
Myo1A>UAS-GFP; Iduna-/-
Myo1A>UAS-Iduna; Iduna-/-

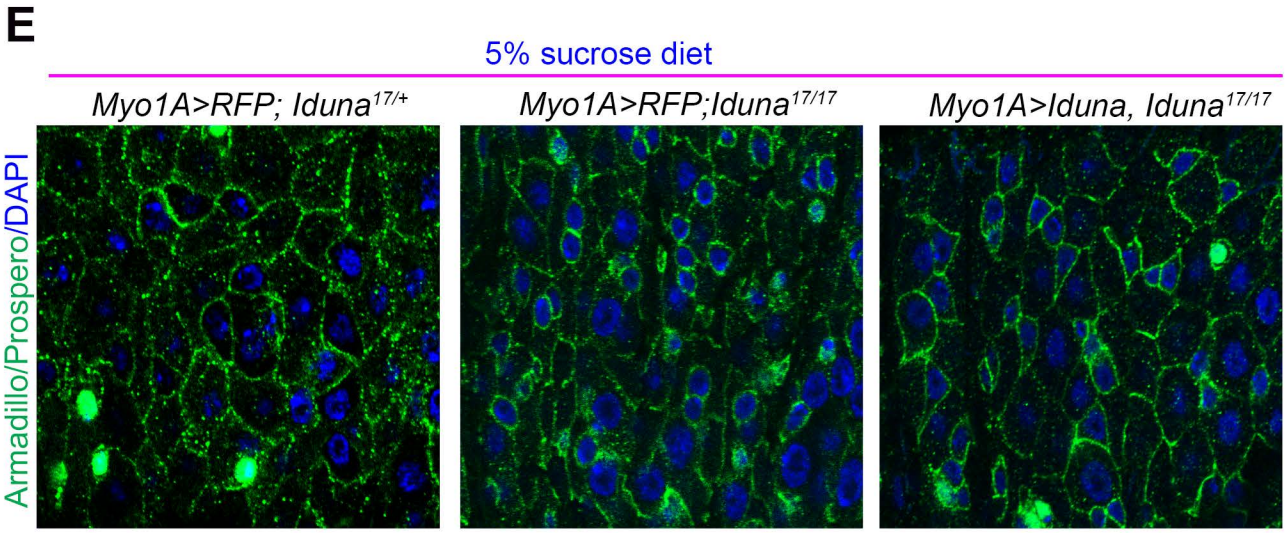
E
5% sucrose diet
Myo1A>RFP; Iduna17/+
Myo1A>RFP;Iduna17/17
Myo1A>Iduna, Iduna17/17
Armadillo/Prospero/DAPI

Figure S6

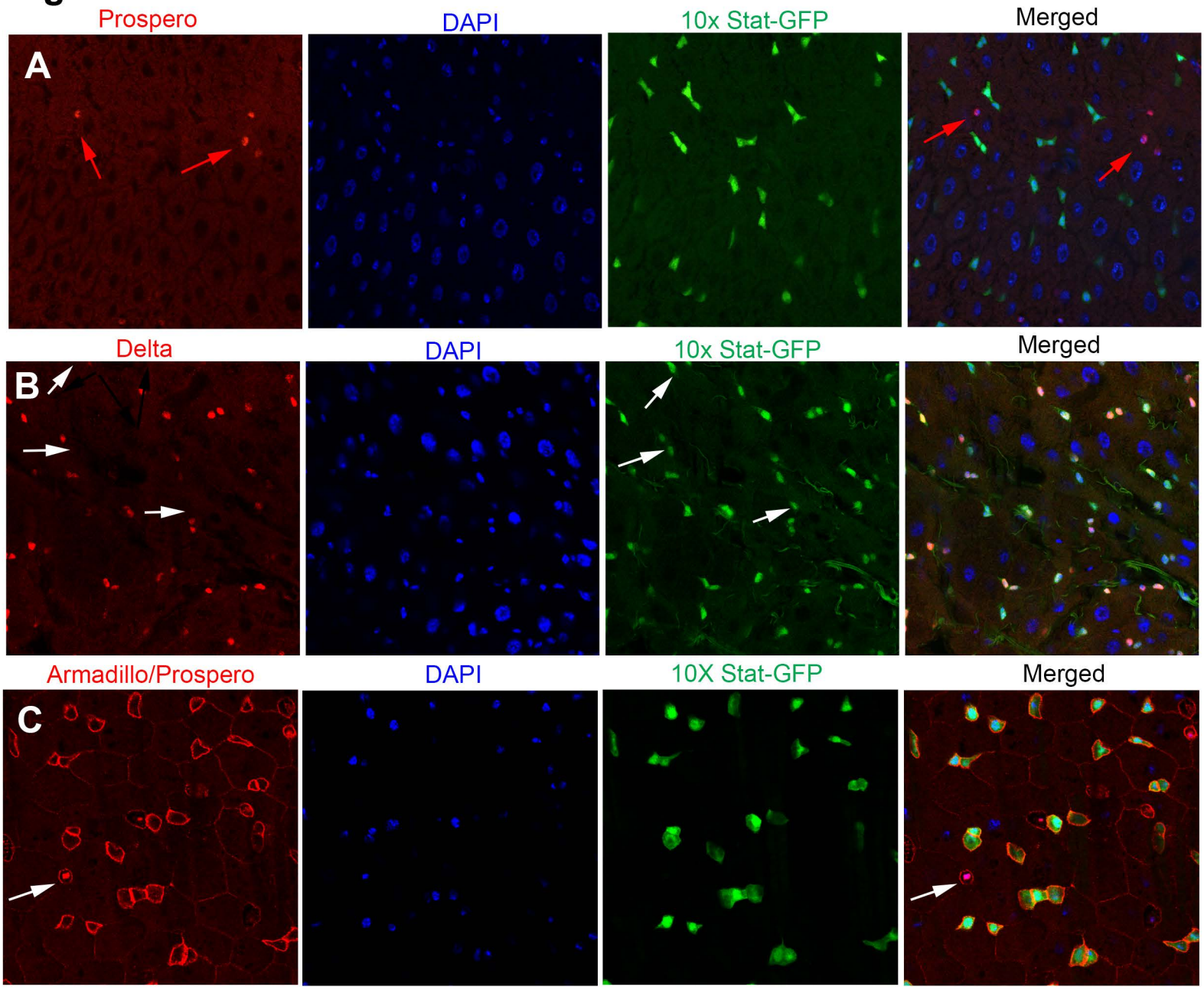
Prospero
DAPI
10x Stat-GFP
Merged
A
Delta
DAPI
10x Stat-GFP
Merged
B
Armadillo/Prospero
DAPI
10X Stat-GFP
Merged
C

Figure S7

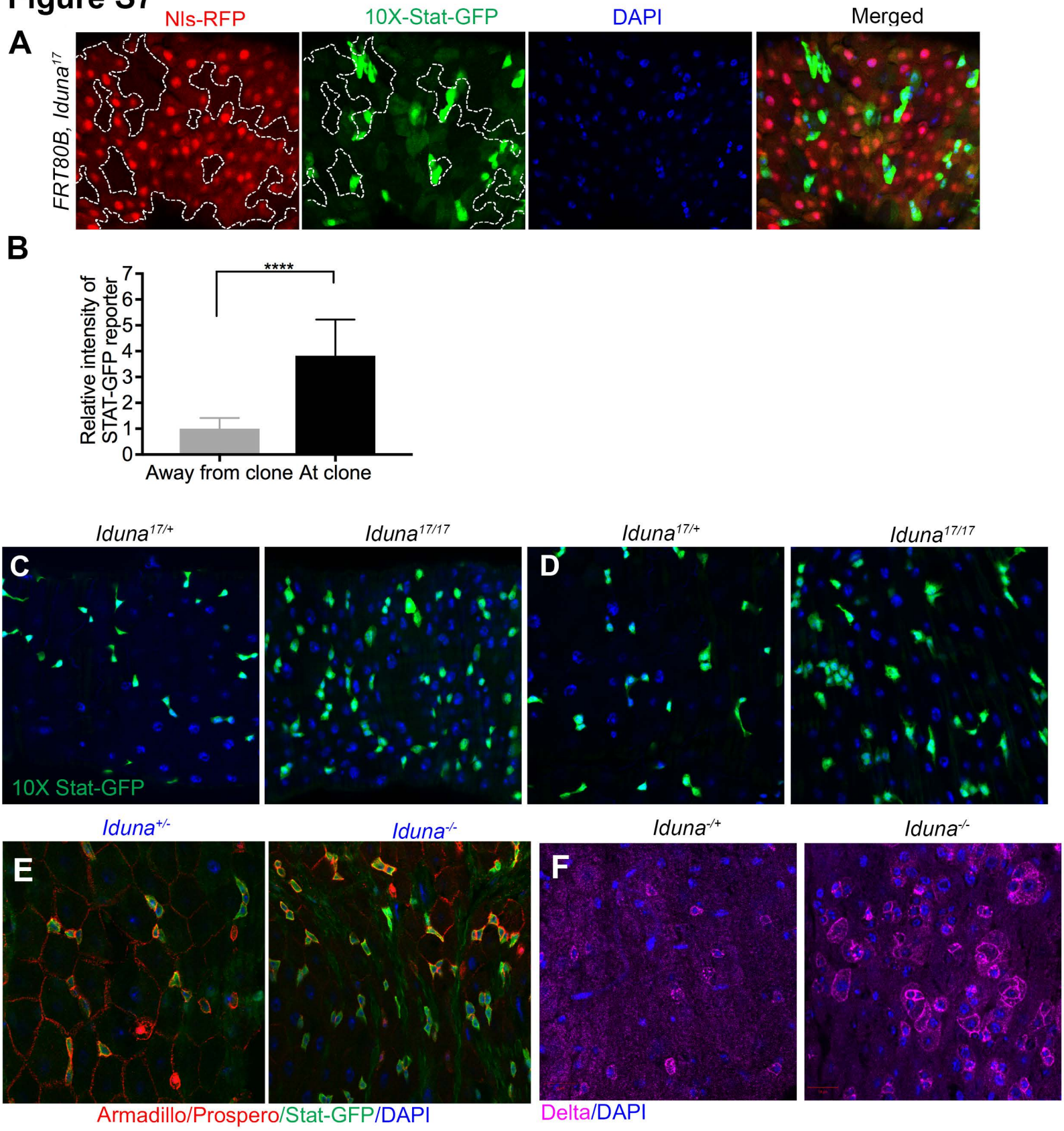
A
Nls-RFP
10X-Stat-GFP
DAPI
Merged
FRT80B, Iduna17
B
****
Relative intensity of STAT-GFP reporter
0
1
2
3
4
5
6
7
Away from clone
At clone
Iduna17/+
Iduna17/17
Iduna17/+
Iduna17/17
C
D
10X Stat-GFP
Iduna+/-
Iduna-/-
Iduna-/+
Iduna-/-
E
F
Armadillo/Prospero/Stat-GFP/DAPI
Delta/DAPI

Figure S8

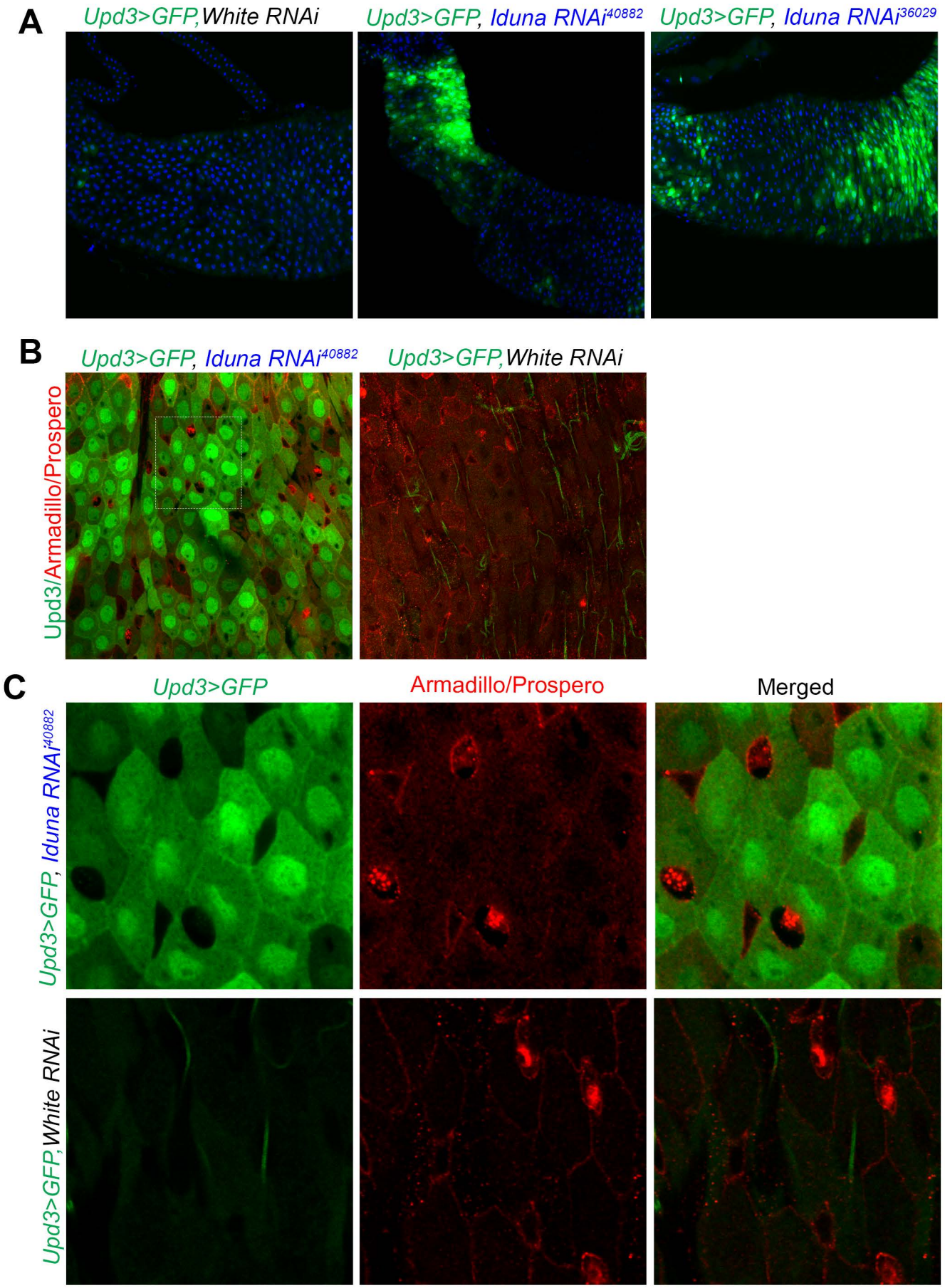
A
Upd3>GFP,White RNAi
Upd3>GFP, Iduna RNAi40882
Upd3>GFP, Iduna RNAi36029
B
Upd3>GFP, Iduna RNAi40882
Upd3>GFP,White RNAi
Upd3/Armadillo/Prospero
C
Upd3>GFP
Armadillo/Prospero
Merged
Upd3>GFP, Iduna RNAi40882
Upd3>GFP,White RNAi